**TITLE**: Modelling dementia in *Drosophila* uncovers shared and specific targets of TDP-43 proteinopathy across ALS and FTD relevant circuits

Authors: R Keating Godfrey[1,2,*], Reed T Bjork[1], Eric Alsop[3], Brijesh S Chauhan[4], Hillary C Ruvalcaba[1], Jerry Antone[3], Allison F Michael[1], Christi Williams[1], Grace Hala'ufia[1], Alexander D Blythe[1], Megan Hall[3], Kendall Van Keuren-Jensen[3], Daniela C Zarnescu [1,4,*]

**AFFILIATIONS**:

[1] Department of Molecular and Cellular Biology, 1007 E. Lowell St, Life Sciences South, University of Arizona, Tucson AZ 85721, USA

[2] current address: McGuire Center for Lepidoptera and Biodiversity, Florida Museum of Natural History, 3215 Hull Road, University of Florida, Gainesville, FL 32611, USA

[3] Translational Genomics Research Institute, 445 N 5th St, Phoenix, AZ 85004, USA

[4] current address: Cellular and Molecular Physiology, 500 University Drive Crescent Building C4605, Penn State College of Medicine, Hershey PA 17033, USA

* corresponding authors: Daniela C Zarnescu dcz102@psu.edu, R Keating Godfrey rkgodfrey@floridamuseum.ufl.edu

**ABSTRACT** (150-200 words)

Amyotrophic lateral sclerosis (ALS) and fronto-temporal dementia (FTD) comprise a spectrum of neurodegenerative diseases linked to TDP-43 proteinopathy, which at the cellular level, is characterized by loss of nuclear TDP-43 and accumulation of cytoplasmic TDP-43 puncta that ultimately cause RNA processing defects including dysregulation of splicing, mRNA transport and translation. Complementing our previous models of ALS, here we report a novel model of FTD based on overexpression of TDP-43 in the *Drosophila* mushroom body (MB) circuit. This model recapitulates several aspects of FTD pathology including age-dependent neuronal loss, and nuclear depletion and cytoplasmic accumulation of TDP-43, accompanied by behavioral deficits in working memory and sleep that occur before axonal degeneration ensues. RNA immunoprecipitations identify several candidate mRNA targets of TDP-43 in MBs, some of which are unique to the MB circuit while others are shared with motor neurons. Among the latter is the glypican Dally-like-protein (Dlp), a modulator of Wg/Wnt signaling. Using genetic interactions we show that overexpression of Dlp in MBs mitigates TDP-43 dependent working memory deficits. These results highlight the utility of modelling TDP-43 proteinopathy in *Drosophila* and provide a novel platform for studying the molecular mechanisms underlying FTD, and potentially uncovering shared and circuit specific vulnerabilities in ALS/FTD.

## INTRODUCTION

Characterized by extensive overlap in cellular pathology, genetic mutations, and molecular markers, amyotrophic lateral sclerosis (ALS) and frontotemporal dementia (FTD) comprise a neurodegenerative disease spectrum affecting multiple subsets of neurons in the spinal cord, motor cortex, cingulate cortex, and frontal and temporal lobes (Arai et al., 2006; Ferrari et al., 2011; Ling et al., 2013; Neumann et al., 2006). Notably, nearly 97% of ALS cases (Mackenzie et al., 2007) and approximately 45% of FTD cases (Cairns et al., 2007) exhibit neurodegeneration with ubiquitin-positive cytoplasmic inclusions that contain transactive response (TAR) DNA binding protein 43 (TDP-43). A number of point mutations in *TARDBP*, the gene encoding TDP-43, have been identified as causative of ALS (Kabashi et al., 2008; Rutherford et al., 2008; Sreedharan et al., 2008) while others have been linked to FTD (Borroni et al., 2009; Chen et al., 2019). Although mutations in at least 20 other genes have been associated with ALS/FTD (Al-Chalabi et al., 2012), the majority of ALS/FTD cases are sporadic.

Substantiating its significance as a marker of pathology, TDP-43 has also been identified as a component of cytoplasmic aggregates in dementias other than FTD, including Alzheimer's disease (AD) (Chang et al., 2015; Josephs et al., 2014b; Rohn, 2008), AD with Lewy body dementia (AD/LBD) (McAleese et al., 2017), Parkinsonism-dementia complex (PDC) (Hasegawa et al., 2007), and hippocampal sclerosis (Amador-Ortiz et al., 2007). Up to 57% of AD cases exhibit TDP-43 positive intracellular inclusions (Josephs et al., 2014a); notably, AD patients with TDP-43 proteinopathy show accelerated disease progression with more severe cognitive impairment (Josephs *et al.*, 2014b; Meneses et al., 2021). In addition to the presence of TDP-43 proteinopathy, dementias such as FTD and AD also share TDP-43 associated cellular pathology, including dystrophic neurites (Mackenzie et al., 2011). Thus, despite differences in underlying genetic risk factors and specific neural populations affected, a large proportion of dementias exhibit overlapping TDP-43 pathology, providing a common entry point for understanding shared mechanisms of neurodegeneration (Gao et al., 2018; Jo et al., 2020).

71 Wild-type TDP-43 is localized primarily to the nucleus where it regulates transcription
72 (Swain et al., 2016) and splicing (Fiesel et al., 2012; Freibaum et al., 2010; Ling et al., 2015;
73 Polymenidou et al., 2011; Tollervey et al., 2011) necessary for nervous system development
74 and function. TDP-43 also shuttles between the nucleus and cytoplasm and has been shown to
75 play a role in axonal and dendritic mRNA localization (Alami et al., 2014; Chou et al., 2018;
76 Fallini et al., 2012), stress granule dynamics (Colombrita et al., 2009; Khalfallah et al., 2018;
77 McDonald et al., 2011) and translation (Altman et al., 2021; Coyne et al., 2017; Lehmkuhl et al.,
78 2021). During severe or prolonged cellular stress and in disease, TDP-43 exits the nucleus and
79 associates with ubiquitin-positive cytoplasmic inclusions (Ramaswami et al., 2013). Indeed,
80 cellular dysfunction and subsequent degeneration associated with TDP-43 pathology have been
81 attributed to both loss-of-function of nuclear TDP-43 (Ling et al., 2015) and cytoplasmic gain-of-
82 function (Walker et al., 2015) whereby cytoplasmic inclusions sequester mRNAs and perturb
83 protein homeostasis (Ramaswami et al., 2013).
84 Following the identification of TDP-43 as a protein of pathological interest in numerous
85 neurodegenerative diseases, model organisms have been critical to understanding the normal
86 biological functions of TDP-43 and how disruption of these functions leads to disease. Despite
87 having diverged from a common ancestor with vertebrates over 600 million years ago (Erwin,
88 2015), the fruit fly (*Drosophila melanogaster*) genome contains a homolog of *TARDBP*, namely
89 *TBPH*, which displays sequence similarity and functional overlap with human TDP-43 (Ayala et
90 al., 2005; Estes et al., 2011).
91 In addition to extensive overlap in neurogenetic homology, circuit-level conservation in
92 the central nervous system has also been demonstrated between invertebrates and vertebrates
93 (Bier, 2005; Bridi et al., 2020; Strausfeld and Hirth, 2013), making invertebrate models relevant
94 for understanding diseases of cognition. Indeed, flies display several behaviors affected in
95 human disease (Muqit and Feany, 2002) including associative learning (Heisenberg, 2003),
96 long-term memory (Isabel et al., 2004), sleep (Shaw et al., 2000), social interactions (Baier et

97 al., 2002; Kamyshev et al., 2002), and addiction (Bellen, 1998) that can serve as system-level
98 readouts of molecular- and/or cellular-level dysfunction. Models of TDP-43 proteinopathy in
99 *Drosophila* have recapitulated the locomotor phenotypes, motor neuron dysfunction, and
100 shortened lifespan (Estes et al., 2011; Li et al., 2010; Romano et al., 2012) observed in ALS and
101 highlighted degeneration in central brain structures (Li et al., 2010) reminiscent of FTD. Beyond
102 simply simulating disease states, these fly models have identified translational targets (Coyne et
103 al., 2017; Coyne et al., 2014; Lehmkuhl et al., 2021) and genetic modifiers of TDP-43
104 proteinopathy (Azpurua et al., 2021; Coyne et al., 2015; Sreedharan et al., 2015; Zhan et al.,
105 2013), and exposed systemic effects on metabolic pathways (Loganathan et al., 2022; Manzo et
106 al., 2019).

107 While TDP-43 proteinopathy has been extensively studied in motor neurons and glia as
108 a model of ALS, a robust fly model of dementia based on TDP-43 proteinopathy has not yet
109 been established. This is in part because the mushroom bodies (MBs) of the fly brain, which
110 were originally described as essential to odor learning (de Belle and Heisenberg, 1994) have
111 only recently been recognized as being required for multi-modal and context-dependent learning
112 (Liu et al., 1999; Vogt et al., 2014) including place learning (Ostrowski et al., 2015). The MBs
113 also regulate sleep (Driscoll et al., 2021; Joiner et al., 2006), satiety (Tsao et al., 2018), social
114 behavior (Sun et al., 2020) and gate behaviors attributed to other brain regions such as
115 decision-making (Zhang et al., 2007) and aggression (Zwarts et al., 2015). Therefore, the MBs
116 share functional overlap with regions of the vertebrate cortex (Wolff and Strausfeld, 2016).
117 Existing fly models of intellectual disability (Mariano et al., 2020) and AD(Chakraborty et al.,
118 2011) have either focused on, or identified phenotypes in the MBs of the fly brain, suggesting
119 that this structure is appropriate for modelling diseases of cognition.

120 Here we describe the development of a novel fly model of FTD based on TDP-43
121 proteinopathy induced by overexpression of wild-type or mutant human TDP-43 in a subset of
122 MB neurons. Our model recapitulates key cellular and behavioral characteristics of human

123 dementias with TDP-43 pathology, including age-dependent loss of nuclear TDP-43, axonal
124 degeneration, and working memory and sleep deficits that parallel those observed in dementia
125 patients. Using RNA immunoprecipitations we show that in MBs, TDP-43 associates with
126 several mRNAs, a subset of which are unique to MBs while others are shared with mRNA
127 targets previously identified in motor neurons. Interestingly, among the latter group we identified
128 *dlp* mRNA, encoding the heparan sulfate proteoglycan (HSPG) Dally-like protein (Dlp)/GPC6,
129 which we previously showed that is a target of TDP-43 in fly models of ALS and altered in ALS
130 spinal cords (Lehmkuhl et al., 2021). We report that *dlp* mRNA is enriched in TDP-43 complexes
131 in MBs and Dlp protein is decreased within axons in an age-dependent manner, consistent with
132 TDP-43 dependent axonal transport and/or translation deficits. Notably, Dlp overexpression in
133 MBs rescues TDP-43 dependent deficits in working memory consistent with Dlp being a
134 physiologically significant target of TDP-43 in the MB circuit. These findings demonstrate that
135 TDP-43 proteinopathy in MBs causes dementia-like phenotypes that are mediated at least in
136 part by the heparan sulfate proteoglycan (HSPG) Dally-like protein (Dlp)/GPC6, a regulator of
137 the Wg/Wnt signaling pathway. Furthermore, we identify candidate targets of TDP-43 unique to
138 MBs that suggest distinct neuronal vulnerabilities across the ALS – FTD spectrum.
139

140 **RESULTS**

141 *Overexpression of TDP-43 in Kenyon cells results in age-dependent cell loss and nuclear to*
142 *cytoplasmic mislocalization*

143 The insect MBs are comprised of large, complex neurons called Kenyon cells, referred
144 herein as MB neurons (MBNs), which form a layered network with reticular feedback
145 (Crittenden, 1998), structural characteristics reminiscent of vertebrate cortical neurons and
146 networks. There are three subtypes of MBNs based on developmental origin, cell morphology,
147 and wiring. Axons of these three types form five layered lobes, the $\alpha/\beta$ , $\alpha'/\beta'$, and $\gamma$ lobes, which
148 are further compartmentalized into columnar-like regions based on neuromodulatory inputs and

149 excitatory or inhibitory postsynaptic partners (Aso et al., 2014). To model FTD-like TDP-43
150 proteinopathy we used a split-GAL4 driver line *SS01276* available from the Janelia FlyLight
151 split-GAL4 driver collection (Aso, 2021) to express human TDP-43 (Estes et al., 2013) in a
152 subset of MBNs that form the α/β and γ lobes of the adult *Drosophila* mushroom bodies.
153 Mushroom body development is well-characterized in *Drosophila* . Neurons forming the γ and
154 α'/β' lobes are embryonic and larval in origin, respectively (Kunz et al., 2012) and persist
155 through metamorphosis, whereas those comprising the α/β lobes are born after puparium
156 formation (Lee et al., 1999).
157 We characterized expression driven by *SS01276* in the 3rd instar larva (L3) and found
158 that cytoplasmic YFP, YFP tagged TDP-43 (*TDP-43::YFP*) and membrane targeted RFP
159 (*mCD8:: RFP*) are limited to MBNs (Figure 1-supplement 1). Signal is detected in approximately
160 50 larval MBNs in both TDP-43$^{WT}$ overexpression (OE) and TDP-43$^{G298S}$ OE brains (Figure
161 1A,1F *TDP-43$^{WT}$::YFP mCD8::RFP*; Figure 1-supplement 2,*TDP-43$^{G298S}$::YFP mCD8::RFP*). In
162 L3, the MBs comprise approximately 60 γ lobe MBNs and 40 α'/β' lobe MBNs (Lee et al., 1999)
163 thus at this stage *SS01276* could possibly be driving expression in some combination of γ lobe
164 or α'/β' lobe MBNs. However, since adult expression of *SS01276* was determined to be limited
165 to γ and α/β lobe MBNs (Aso, 2021), and given that both γ and α'/β' lobe MBNs persist through
166 metamorphosis, it is likely that the expression we observed during L3 for *SS01276* corresponds
167 to γ lobe MBNs.
168 Visual inspection of larval MBNs indicated that TDP-43 YFP was largely confined to the
169 nucleus in L3 brains (Figure 1A) but became mislocalized outside the nucleus in young adults.
170 The nucleus comprises nearly all of the cell body in MBNs, making it challenging to accurately
171 assess cytoplasmic mislocalization or nuclear depletion. Therefore, to determine age-dependent
172 changes in TDP-43 localization, we measured mean signal intensity of TDP-43 YFP in the
173 nucleus by tracing the nucleus in the Hoechst channel, then measured mean signal intensity of

174 TDP-43 YFP in the entire cell by tracing the YFP signal of the entire cell boundary (see
175 Materials and Methods and Figure 1-supplement 3) and calculated the ratio of nucleus to total
176 cell signal mean intensity (Figure 1D, E). Since the MBN cytoplasms are extremely thin, this
177 ratio should be nearly 1.0 when TDP-43 is localized to both the nucleus and the cytoplasm
178 (single arrow, Figures 1B, D), less than 1.0 when TDP-43 YFP is depleted from the nucleus and
179 mislocalized to the cytoplasm (see double arrows, Figures 1B, D) and slightly above 1.0 when
180 TDP-43 is contained largely in the nucleus (see stacked arrows, Figures 1C, D).

181 Using this measure of nuclear depletion, we found a significant decrease in the mean
182 signal intensity ratio across the population of MBNs from juvenile to young adults in the context
183 of both TDP-43 OE variants (Figure 1E, *TDP-43$^{WT}$::YFP mCD8::RFP* 0.978$\pm$0.005 in L3 vs.
184 0.869$\pm$0.009 in young adults, P < 0.0001; Figure 1-supplement 2, *TDP-43$^{G298S}$:: YFP*
185 *mCD8::RFP* 0.967$\pm$0.002 in L3 vs 0.906$\pm$0.012 in young adults, P = 0.0004; supplemental
186 table S1E). Surprisingly, the ratio of nucleus to total cell signal mean intensity increased in old
187 adult brains compared to young adults, however, it was still significantly lower than at the
188 juvenile age time point (L3) in our TDP-43$^{WT}$ OE model (Figure 1E, 0.978$\pm$0.005 in L3 vs.
189 0.927$\pm$0.009 in old adults, P = 0.0041; supplemental table S1E). A plausible explanation for this
190 result is provided by our findings that there are significantly fewer TDP-43 YFP positive MBNs in
191 old compared to younger TDP-43 OE brains or to old YFP controls (*TDP-43$^{WT}$:: YFP*
192 *mCD8::RFP,* 445$\pm$96 cells in old adults vs 1089$\pm$40 cells in young adults vs. 1206$\pm$150 cells in
193 YFP old adults, P < 0.001; Figure 1F). Similar results were obtained for TDP$^{G298S}$ YFP
194 expressing brains (*TDP-43$^{G298S}$:: YFP mCD8::RFP* 473$\pm$79 cells in old adults vs 1097$\pm$55 cells
195 in young adults vs 1206$\pm$150 cells in YFP old adults, P < 0.001; Figure1-supplement 2;
196 supplemental table S1F). These results are consistent with TDP-43 OE causing age-dependent
197 cell loss and suggest that the MBNs exhibiting increased levels of cytoplasmic TDP-43 are more
198 vulnerable and lost during aging, likely through increased cell death.

199

200 *Mushroom body axons exhibit age-dependent TDP-43 puncta accumulation and progressive*
201 *degeneration*

202 To determine the effect of TDP-43 proteinopathy on axonal integrity and overall lobe
203 morphology, we co-expressed TDP-43 and the membrane marker mCD8 RFP. Signal intensity
204 of mCD8 RFP showed progressive decrease in the γ lobe over time (young, 1.01±0.04, middle-
205 aged, 0.87±0.25, and old, 0.40±0.10 fluorescence intensity ratio to age matched controls;
206 Figure 2A, B, insets b, e, h; quantified in C; supplemental table S2A), suggesting that axonal
207 thinning occurred in an age-dependent manner. Simultaneously, TDP-43 formed increasingly
208 larger axonal puncta in the γ lobe with age (young, 1.00±0.04, middle-aged, 1.19±0.05, and old,
209 1.35±0.05 area normalized to age matched controls Figure 2B, insets c, f, i; quantified in D;
210 supplemental table S2B). These findings are consistent with the formation of dystrophic axons,
211 membrane fragmentation and cytoplasmic aggregation of TDP-43. A similar pattern of axonal
212 loss and fragmentation in the γ lobe, coincident with increased TDP-43 puncta size, was
213 observed in TDP-43$^{G298S}$ OE flies (Figure 2-supplement 1A, B insets c, f, i, quantified in C and
214 D; supplemental tables S2A, S2B). We could not detect statistically significant changes in
215 mCD8 RFP signal intensity nor TDP-43 cytoplasmic puncta in the α/β lobes of TDP-43$^{WT}$ OE
216 flies, however these lobes showed dramatic, age-dependent thinning not observed in controls
217 (Figure 2B inset i). In TDP-43$^{G298S}$ OE brains, we observed both an increase in the size of TDP-
218 43 YFP cytoplasmic puncta within α/β lobes between young and middle-aged adults, and a
219 thinning of these lobes (Figure 2-supplement 1B inset i). Interestingly, these phenotypes are
220 reminiscent of the age-dependent pathophysiology observed in human patients. Given that γ
221 lobe neurons are born earlier than those within the α/β lobes, the more severe phenotypes
222 observed in this neuronal subpopulation highlight the potential contribution of aging to TDP-43
223 proteinopathy.

224

225 *TDP-43 proteinopathy causes working memory deficits*

226 In humans, working memory is disrupted in FTD and other TDP-43 associated
227 dementias (Poos et al., 2018; Stopford et al., 2012). To test whether flies overexpressing TDP-
228 43 exhibit working memory deficits, we used miniature Y-mazes to measure spontaneous
229 alternation behavior by scoring the number of three consecutive arm entries over a period of ten
230 minutes (see Materials and Methods, Figure 3A, Lewis et al., 2017). These experiments showed
231 that although TDP-43 OE results in increased overall movement (males: *TDP-43$^{WT}$::YFP* in an
232 *Oregon-R background*, 146.00$\pm$7.51 mm vs. *Oregon-R*, 106.19$\pm$8.18 mm, P = 0.018; females:
233 *TDP-43$^{WT}$::YFP* in an *Oregon-R background*, 110.53$\pm$7.51 mm vs. *Oregon-R*, 81.12$\pm$5.24 mm;
234 Figure 3B; for means of individual replicates see supplemental table S3), percent alternation is
235 significantly decreased in young adult males (*TDP-43$^{WT}$::YFP* in an *Oregon-R background*,
236 0.57$\pm$0.01 vs. *Oregon-R*, 0.61$\pm$0.01, P = 0.012) and females (*TDP-43$^{WT}$::YFP* in an *Oregon-R*
237 *background*, 0.60$\pm$0.02 vs. *Oregon-R*, 0.65$\pm$0.01, P = 0.006; Figure 3C), consistent with TDP-
238 43 proteinopathy causing working memory deficits in the MB circuit.

239

240 *TDP-43 expression in the MB circuit causes sleep alterations*

241 In humans, frontal and temporal lobe degeneration is associated with increased daytime
242 somnolence (Sani et al., 2019), but overall sleep disturbances are highly variable in FTD and
243 may be detectable in earlier stages than in AD (Bonakis et al., 2014). To determine whether
244 TDP-43 proteinopathy in the MB circuit alters sleep, we used *Drosophila* Activity Monitors
245 (DAMs, see Materials and Methods) to measure total daytime and nighttime sleep. Our
246 experiments show that on average, both male and female TDP-43 OE flies appear to be
247 lethargic; they spent a greater proportion of their time sleeping during both the day and night
248 compared to controls (approximately 11% more for TDP-43$^{WT}$ OE and approximately 8% more
249 for TDP-43$^{G298S}$ OE). However, there are subtle differences in how TDP-43 OE affects sleep

250 patterns based on age and sex. While males consistently sleep more during the day, this effect
251 is weaker in females flies where we found trends towards increased daytime sleep at some but
252 not all age time points in each genotype (Figure 4A; supplemental table S4A). At night, males
253 and females also exhibited a general tendency towards increased sleep with the exception of
254 young TDP-43 OE adult males which, when compared to $w^{1118}$ controls, showed signs of sleep
255 fragmentation as evidenced by more frequent, shorter sleep bouts (Figures 4B, C for TDP-43$^{WT}$
256 OE and Figure 4-supplement 1B, C for TDP-43$^{G298S}$ OE*;* supplemental tables S4C sleep bout
257 length and S4C sleep bout number).

258 Interestingly, both humans and flies show decreased nighttime sleep with age (Li et al.,
259 2018); in line with this, $w^{1118}$ flies of both sexes showed age-related declines in nighttime sleep,
260 whereas TDP-43 OE males showed no such declines (all pairwise comparisons $P > 0.05$) and
261 female declines appear less steep (TDP-43$^{WT}$ OE, Figure 4B; TDP-43$^{G298S}$ OE, Figure 4-
262 supplement 1; supplemental tables S4A), consistent with our findings that TDP-43 proteinopathy
263 causes lethargy. By middle age, TDP-43$^{WT}$ OE males showed a pattern of longer, less frequent
264 nighttime sleep bouts as compared with $w^{1118}$ (Figure 4C). Within each genotype, female $w^{1118}$
265 and TDP-43$^{WT}$ OE flies exhibited age-related sleep fragmentation as evidenced by a greater
266 number of shorter bouts at 60 - 63 days compared with 1 – 3 days. TDP-43 OE flies still spent a
267 greater proportion of their time sleeping than controls (Figure 4B; supplemental table S4A), an
268 effect driven by longer sleep bouts at this aged time point (Figure 4C; supplemental table S4C).
269 Taken together, these results indicate that TDP-43 OE in the MB circuit causes sleep deficits
270 resembling those reported in FTD patients, including increased sleep during the day and sleep
271 fragmentation at night, albeit the latter was detected in young males only. Notably, the sleep
272 fragmentation phenotype occurs concomitant with the nuclear depletion of TDP-43 and before
273 axonal degeneration suggesting that this may be a direct consequence of TDP-43
274 mislocalization while lethargy is likely an indirect consequence of large-scale neuronal
275 degeneration.

276

277 *TDP-43 overexpression in Kenyon cells is sufficient to reduce lifespan in Drosophila*

278 Life expectancy for FTD patients after diagnosis is approximately 8 – 12 years and, while
279 patients do not often die from the disease itself, there is a measurable, if subtle, effect on life
280 expectancy (Kansal et al., 2016; Loi et al., 2021). We therefore tested whether TDP-43
281 proteinopathy affects lifespan in our fly model and found that overexpression of TDP-43 in
282 MBNs significantly reduces median survival time (TDP-43$^{WT}$ OE, 84 days, 95% CI [84,84]; TDP-
283 43$^{G298S}$ OE, 89 days, 95% CI [88,91]) when compared with *YFP* controls (94 days, 95% CI [90,
284 95]; $P < 0.0001$ and $P = 0.028$, respectively; Figure 5 and Figure 5-supplement 1). These results
285 indicate that overexpression of TDP-43 in a subset of MBNs in flies is sufficient to produce a
286 nearly 10% reduction in median lifespan.

287

288 *mRNAs enriched with TDP-43 in mushroom body neurons show partial overlap with those*
289 *previously identified in motor neuron and include components of the Wnt/Wg signaling pathway*

290 To understand how TDP-43 overexpression influences the MBN proteome, we
291 immunoprecipitated YFP-tagged TDP-43$^{WT}$ or TDP-43$^{G298S}$ from *Drosophila* heads
292 overexpressing TDP-43 YFP in MBNs using the *SS01276* Split-GAL4 driver. Next, we used
293 DESeq2 (Love et al., 2014) to assess differential expression of mRNAs enriched in TDP-43
294 complexes compared to the whole brain transcriptome. We chose to identify TDP-43-enriched
295 candidate mRNA targets using young adult flies (1 – 3 days post-eclosion), before age-
296 dependent axonal neurodegeneration is detected in the MB lobes, to avoid detection of gene
297 expression alterations that could be an indirect consequence of neurodegeneration. Of the
298 13,302 transcripts detected in the fly brain, we identified 1055 and 1393 candidate mRNA
299 targets based on their enrichment in TDP-43$^{WT}$ YFP and TDP-43$^{G298S}$ YFP complexes,
300 respectively (Log2FC > 1 compared to the brain transcriptome, $P_{adj} < 0.05$ ) (Figure 6A, Figure
301 6-supplement 1A). A total of 876 candidate mRNAs were shared by both variants (83% of

302 targets in TDP-43$^{WT}$ OE and 63% of targets in TDP-43$^{G298S}$ OE), for a total of 1572 mRNAs
303 enriched across both models (with 179 unique to TDP-43$^{WT}$ OE and 517 to TDP-43$^{G298S}$ OE,
304 respectively). Notably, differential expression analyses also recovered previously identified
305 TDP-43 target mRNAs including *futsch* (TDP-43$^{WT}$ OE Log2FC = 1.81, $P_{adj}$ = 2.66E-07; TDP-
306 43$^{G298S}$ OE Log2FC = 2.14, $P_{adj}$ = 9.57E-10) (Coyne et al., 2014) and *dscam2* (TDP-43$^{WT}$ OE
307 Log2FC = 1.29, $P_{adj}$ = 6.01E-04; TDP-43$^{G298S}$ OE Log2FC = 1.81, $P_{adj}$ = 2.42E-3) (Xiao et al.,
308 2011).

309 While TDP-43 has been found to regulate mRNA processing in a cell type specific
310 manner, there is also overlap among TDP-43 splicing targets in neuronal and muscle cell lines
311 (Susnjar et al., 2022). Consistent with these findings, we found that nearly 44% of TDP-43$^{WT}$ OE
312 and 42% of TDP-43$^{G298S}$ OE highly associated mRNAs in MBNs overlapped with those we
313 identified previously in motor neurons (MNs) when modelling ALS by overexpressing TDP-43
314 with the D42 GAL4 driver (Figure 6B, Figure 6-figure supplement 1C).

315 Functional annotation of mRNA candidate targets in the MBs identified neuron-specific
316 as well as neuromuscular junction molecular pathways in both the TDP-43$^{WT}$ OE and TDP-
317 43$^{G298S}$ OE models (Figure 6-supplement 2A). Components of the Wingless (Wg/Wnt) signaling
318 pathway were overrepresented in the TDP-43 proteinopathy model of FTD (Figure 6-
319 supplement 2B). Highly enriched members of these pathways include *frizzled* (*fz*), a Wg/Wnt
320 receptor, *dally-like protein* (*dlp*), a heparan sulfate proteoglycan (HSPG) that interacts with
321 multiple Wnt ligands (Waghmare et al., 2020), and the Wg/Wnt receptor *frizzled 2* (*fz2*) (Yan et
322 al., 2009). Interestingly, *dlp* mRNA was also found to be enriched with TDP-43 in fly motor
323 neurons, where TDP-43 proteinopathy causes depletion of Dlp from the neuromuscular junction
324 and simultaneous accumulation of Dlp puncta in cell bodies (Lehmkuhl et al., 2021). To validate
325 that *dlp* mRNA is a target of TDP-43 in MBNs as predicted by RNA seq, we used RNA IPs
326 followed by RT-qPCR and confirmed that *dlp* mRNA is enriched in immunoprecipitated TDP-
327 43$^{WT}$ and TDP-43$^{G298S}$ complexes compared to input (Figure 6-supplement 1).

328 Among the mRNAs enriched with TDP-43 in fly MBNs we identified several orthologs of
329 human genes exhibiting altered expression in the frontal cortices of FTD patients including the
330 Ras family member RHOQ (*Rac2*, *TDP-43*$^{WT}$ Log2FC = 3.68, $P_{adj}$ = 9.66E-24), the glypican
331 GPC4 (*dlp*, *TDP-43*$^{WT}$ Log2FC =3.33, $P_{adj}$ = 9.14E-23), heat shock 70kDa protein 2, HSPA2
332 (*Hsp70Bb*, *TDP-43*$^{WT}$ Log2FC = 2.77, $P_{adj}$ = 1.59E-7), and the frizzled family receptor protein
333 FZD7 (*fz*, *TDP-43*$^{WT}$ Log2FC = 2.18. $P_{adj}$ = 4.25E-12) (Santiago et al., 2020).
334 In addition to TDP-43 candidate targets shared in MB and MN circuits, we also assessed
335 the pool of mRNAs significantly enriched with TDP-43 in MBNs only, higlighting circuit specific
336 aspects of TDP-43 proteinopathy. For TDP-43$^{WT}$ OE we found 461 enriched mRNAs that are
337 shared in both MB and MN, and 594 mRNAs uniquely enriched in MBs (Figure 6). DAVID
338 analyses of the unique candidate targets for TDP-43$^{WT}$ OE in MBs uncovered several kegg
339 pathways altered in the context of TDP-43 proteinopathy including “Basal transcription factors”,
340 “RNA polymerase”, “Ribosome biogenesis” and “Spliceosome” (supplemental table S6A). For
341 TDP-43$^{G298S}$ we found 592 enriched mRNAs that are shared in both MB and MN, and 802
342 mRNAs uniquely enriched in MBs (Figure 6-supplement 1). DAVID analyses of TDP-43$^{G298S}$
343 specific targets in the MB circuit revealed several significantly represented pathways including
344 “mTOR signaling pathway”, “Other types of O-glycan biosynthesis”, “TGF-beta signaling
345 pathway”, “Nicotinate and nicotinamide signaling pathway”, “Autophagy”, “Nucleotide
346 metabolism” and “Spliceosome” (supplemental table S6B).
347 Taken together, these results show that while some mRNAs enriched with TDP-43 in the
348 MB circuit are specific to MBNs, others are shared with MNs and highlight the Wg/Wnt signaling
349 pathway as a functional target of TDP-43 proteinopathy across the ALS/FTD spectrum.
350
351 *TDP-43 proteinopathy causes severe age-related loss of Dally-like protein in MBNs*
352 Given *dlp* mRNA’s enrichment with TDP-43, we hypothesized that the expression of Dlp protein,
353 a Wg/Wnt regulator, may be affected in MBNs, as we previously found in motor neurons

354 (Lehmkuhl et al., 2021). While Dlp has been shown to be highly expressed in developing MBN
355 axons, where it is thought to be involved in axon guidance (Rawson et al., 2005), its expression
356 and function in adult MBNs has not been characterized. We found that, despite *dlp* mRNA being
357 enriched in TDP-43 complexes in young adult brains, the levels and distribution of Dlp protein in
358 TDP-43 OE flies are comparable with controls at that age (Figures 7A, B). Interestingly, Dlp
359 levels decline with age in both controls and TDP-43 OE flies, however while Dlp is still visible in
360 control fly brains at 50 days, Dlp is nearly undetectable in the brains of TDP-43 OE flies (Figures
361 7A, B, $P < 0.05$). A similar age-dependent reduction in Dlp expression was also detected in the
362 context of TDP-43$^{G298S}$ OE in MBNs (Figure 7-supplement 1). These findings are consistent with
363 *dlp* mRNA being a target of TDP-43 in MBNs and suggest mRNA localization and/or translation
364 as possible mechanisms for the observed reduction in Dlp protein expression.
365
366 *Dlp overexpression rescues TDP-43 dependent working memory deficits*
367 We next evaluated the physiological significance of *dlp* mRNA as a target of TDP-43 in
368 MBs. To address this, we tested whether overexpression of *dlp* mRNA (dlp OE) in the context of
369 TDP-43 proteinopathy could mitigate TDP-43 dependent working memory deficits. Using the Y-
370 maze working memory assay we found that the percent alternation deficits displayed by TDP-
371 43$^{WT}$ OE flies could indeed be mitigated by dlp OE in MBNs (Figure 7D). To account for altered
372 movement caused by TDP-43 OE (*TDP-43$^{WT}$::YFP,* 147.52 $\pm$ 13.52 mm, *w$^{1118}$,* 229.89 $\pm$ 7.43
373 mm, $P < 0.0001$, see Figure 7C), we also compared distance-scaled alternations across
374 genotypes and found that TDP-43 dependent alternation deficits were still mitigated by dlp OE
375 *(TDP-43$^{WT}$::YFP T,* 0.0221 $\pm$ 0.0028 alternation/mm, *TDP-43$^{WT}$::YFP dlp OE,* 0.0286 $\pm$ 0.0036
376 alternation/mm, $P < 0.0001$) while no significant difference was detected between co-
377 overexpression of TDP-43 and Dlp, and dlp OE alone (*TDP-43$^{WT}$::YFP dlp OE,* 0.0286 $\pm$ 0.0036
378 alternation/mm, *dlp OE,* 0.0252 $\pm$ 0.0032 alternation/mm, $P > 0.05$, not shown). We note that
379 although total movement in the Y-maze assay is influenced by the genetic background (*w$^{1118}$*

380 versus *OR-R*, compare Figures 3B and 7C), the significant reduction in spontaneous alternation
381 is consistent in TDP-43 OE flies in both cases (Figures 3C and 7D). These experiments indicate
382 that dlp OE in the MB circuit mitigates TDP-43$^{WT}$ OE dependent working memory deficits as
383 evidenced by the rescue of alternation behavior in the Y-maze assay. Notably, this rescue effect
384 is not due to reduced TDP-43 expression or to diluted GAL4 activity by the presence of an
385 additional UAS promoter, as evidenced by similar TDP-43 levels with or without dlp OE (Figures
386 7-supplement 2, supplement 3). Surprisingly, OE of TDP-43$^{G298S}$ in MBNs did not cause a
387 significant spontaneous alternation phenotype (see raw data in Supplemental Table 7). Taken
388 together, these findings support the notion that *dlp* mRNA is a functional target of TDP-43 *in*
389 *vivo* and mediates, at least in part, TDP-43 dependent, FTD relevant phenotypes in *Drosophila* .
390

391 **DISCUSSION**

392 Neurodegenerative diseases have historically been classified by shared symptomology
393 and post-mortem pathology. More recently, the integration of molecular markers and genetic
394 testing has uncovered evidence that cell-type susceptibility and dysregulation of specific
395 molecular pathways can interact to produce similar clinical presentations across different
396 disease etiologies (Pennington et al., 2011). These findings highlight convergent
397 pathomechanisms during the degeneration process (Gao et al., 2018; Ling et al., 2013) and
398 suggest inroads for better understanding of these complex diseases.

399 A common pathological feature of several neurodegenerative diseases including ALS,
400 FTD and other dementias is the nuclear depletion of the RNA binding protein TDP-43
401 accompanied by the accumulation of cytoplasmic, ubiquitinated foci (Mackenzie et al., 2010)
402 (Amador-Ortiz et al., 2007; Chang et al., 2015; Josephs et al., 2014b; McAleese et al., 2017;
403 Rohn, 2008). Since these dementias are often confirmed post-mortem by the presence of TDP-
404 43 pathology, animal models play an important role in elucidating the molecular mechanisms
405 underlying TDP-43 proteinopathy and its role in neurodegeneration. Among these, fly models

406 have proven their utility in this research landscape in part because the availability of powerful
407 molecular and genetic tools allowing multiple hypotheses to be pursued in parallel on a large
408 scale. Indeed, fly models of TDP-43 proteinopathy based on loss of function or overexpression
409 in the entire nervous system (Feiguin et al., 2009; Lu et al., 2009; Romano et al., 2012), or in
410 subsets of neurons including associative regions of the central brain (Li et al., 2010),
411 motoneurons (Estes et al., 2011) or the retina (Elden et al., 2010) have revealed a broad
412 repertoire of altered pathways that have subsequently been confirmed in patient tissues (Coyne
413 et al., 2017; Coyne et al., 2014; Lehmkuhl et al., 2021).

414 It has been previously shown that overexpression of TDP-43 in all MBNs using the driver
415 line OK107 GAL4 (RRID:BDSC_854) caused age-dependent cell loss and axonal degeneration
416 in MBs, however degeneration severity varied widely across nearly isogenic individuals,
417 challenging its utility as a disease model (Li et al., 2010). This variability could be in part
418 attributed to driver line “leakiness” as OK107 GAL4 drives expression beyond MBs, in optic lobe
419 neuropils (Aso et al., 2009; Morante and Desplan, 2008) and neurosecretory cells (Enell et al.,
420 2010; Hampel et al., 2011).To develop a robust and MB specific model of TDP-43 driven
421 dementia in *Drosophila melanogaster,* we leveraged a split-GAL4 driver line with limited
422 expression to a subset of Kenyon cells ($\gamma$, $\alpha/\beta$ MBNs). Notably, this model exhibits nuclear
423 depletion and cytoplasmic accumulation of TDP-43, accompanied by age-dependent axonal
424 degeneration and cell loss, all of which recapitulate key aspects of disease pathology.
425 Importantly, the onset of FTD relevant behavioral symptoms is detectable prior to widespread
426 degeneration, as observed in human disease. Additionally, this model identifies both novel, MB
427 specific, and motor neuron-shared mRNA candidate targets that have previously been
428 associated with TDP-43 pathology. Of the latter, here we chose to focus on the glypican Dlp, a
429 Wg/Wnt signaling regulator and show that Dlp is a functional target of TDP-43 in the MB circuit
430 that mediates, in part, TDP-43 dependent working memory deficits in the fly model.

431 Neurodegeneration in ALS/FTD is thought to be driven by both loss of nuclear function,
432 as some nuclei become devoid of TDP-43, and cytoplasmic gain of toxic function, as evidenced
433 by TDP-43 accumulation in cytoplasmic puncta. While thus far invertebrate models of TDP-43
434 proteinopathy have not faithfully recapitulated TDP-43 mislocalization (e.g., Ash et al., 2010;
435 Estes et al., 2013), here we found that TDP-43 overexpression in MBNs more closely resembles
436 disease pathology. Indeed, TDP-43 displays normal localization in the juvenile stage but
437 becomes depleted from the nucleus and mislocalized to the cytoplasm in young adults.
438 Although changes in TDP-43 localization could reflect developmental regulation (Park et al.,
439 2020), our finding that the number of cells with increased cytoplasmic TDP-43 is reduced from
440 young to old age concomitant with an overall reduction in MB neuron numbers, suggests that
441 cytoplasmic TDP-43 is toxic.
442 Axonal degeneration is evident only in older adult flies and differentially affects MBNs
443 that form the $\alpha/\beta$ and $\gamma$ lobes, with the latter showing the greatest degeneration severity. This is
444 particularly interesting because MBNs that form the $\gamma$ lobe are embryonic in origin and therefore
445 older than the pupal-born MBNs that form the $\alpha/\beta$ lobes (Ito et al., 1997; Kunz et al., 2012; Yu
446 and Lee, 2007), highlighting the aging component of neurodegeneration. It is also possible that
447 the differences in the onset and effects of TDP-43 proteinopathy we observed in $\gamma$ lobe MBNs
448 may be due to their remodelling during metamorphosis (Kunz et al., 2012), which may increase
449 their vulnerability to TDP-43. Taken together, these findings parallel differential susceptibility
450 observed in human cortical neurons (Nana et al., 2019; Seeley, 2008). Given the availability of
451 split-GAL4 driver lines for subsets of MBNs (Aso et al., 2014) future studies could focus on
452 better understanding what drives this susceptibility by modelling TDP-43 proteinopathy in
453 various neuronal subpopulations within the MB circuit. It will be interesting to combine these
454 powerful genetic tools with single cell RNA seq efforts in patients and flies in order to pinpoint
455 specific cell sub-types that may be more vulnerable.

456 Frontotemporal lobar degeneration with TDP-43 proteinopathy (FTLD-TDP) is
457 pathologically classified based on the cortical layers affected, the number of dystrophic neurites,
458 and the extent of neuronal cytoplasmic inclusions (Mackenzie et al., 2011). This pathology is
459 also commonly observed in AD/LBD that exhibit TDP-43 proteinopathy, although different brain
460 regions are selectively affected (Josephs et al., 2014a; Josephs et al., 2014b). Interestingly, we
461 find that neuronal cytoplasmic inclusions are absent in juveniles, appear first in young adult
462 brains and increase in size during aging. This neuropathology precedes observations of
463 dystrophic neurites, which are first visible around middle age, increase in severity during aging,
464 and ultimately degenerate. This age-dependent pathology observed in the fly brain parallels that
465 observed in human disease and provides a platform for studying the progression of
466 neurodegeneration in the genetically tractable *Drosophila* model.
467 In humans, behavioral symptoms of FTD precede widespread degeneration by years
468 suggesting that behavioral deficits arise prior to neuronal pathology, in the absence of complete
469 loss of nuclear TDP-43 function or cytoplasmic accumulation (Perry et al., 2017). Therefore, we
470 chose to focus primarily on working memory and sleep deficits using young adult flies, in which
471 a subset of MBNs show nuclear depletion accompanied by widespread TDP-43 mislocalization
472 to the axonal cytoplasm while MBN axons still appear largely intact. At this young age, we found
473 both working memory and sleep fragmentation phenotypes, albeit the latter were only significant
474 in males. We also assessed these behaviors in aged flies, however the distinct age-dependent
475 deficits exhibited by the controls themselves confounded the detection of TDP-43 specific
476 phenotypes.
477 Behavioral variant frontotemporal dementia (bvFTD) is diagnosed based on often subtle
478 behavioral symptoms including a lack of empathy, increased apathy and compulsive behaviors,
479 and deficits in executive function (Rascovsky et al., 2011). FTD was classically distinguished
480 from AD using a perceived lack of memory deficits, however recent patient studies and meta-
481 analyses indicate that memory deficits are common in bvFTD and at times indistinguishable

482 between AD and bvFTD (Graham et al., 2005; Pennington et al., 2011), challenging the validity
483 of the exclusion of episodic memory deficits in the clinical diagnoses of bvFTD (Hornberger and
484 Piguet, 2012). Although sleep symptoms are notoriously variable and understudied across
485 different FTD diagnoses, the most common sleep disturbances observed in bvFTD patients are
486 sleep fragmentation and daytime sleepiness that may or may not be accompanied by insomnia
487 (Bonakis et al., 2014; McCarter et al., 2016; Sani et al., 2019). Our findings of limited sleep
488 fragmentation and daytime sleepiness highlight potential differences between the fly model and
489 human disease presentation. That said, the limited yet specific deficits caused by TDP-43 OE in
490 MBNs provide a robust measurable sleep disruption that can serve as an organism-level output
491 for future molecular or pharmacological intervention experiments.

492 In addition to observed behavioral deficits, flies with TDP-43 proteinopathy show an
493 approximately 10% reduction in median lifespan. This may be roughly comparable to human
494 patients where FTD exerts a subtle effect on lifespan. In humans, mean age at diagnosis is 61.9
495 for early onset disease (< 65 years) with mean survival after diagnosis around 8 years (Kansal
496 et al., 2016), meaning survival is reduced in comparison with the general population in most
497 countries were clinical data are collected (e.g., 78.8 years in the United States Murphy et al.,
498 2021). Effects on lifespan may be far more severe than a simple comparison of life expectancy
499 would indicate, as Loi et al. (2021) report an increase in mortality risk for FTD patients when
500 compared with age-matched controls. From the perspective of a fly model, it is somewhat
501 surprising to see a lifespan effect given that MBNs comprise a small fraction of total neurons in
502 the fly brain and are often thought to be largely dispensable for viability (de Belle and
503 Heisenberg, 1994). There is evidence that lifespan is regulated at least in part by the $\alpha/\beta$ MBNs
504 (Lien et al., 2020), a subset of MBNs included in our model, however loss of key MB proteins
505 such as DCO (Yamazaki et al., 2007) or overexpression of vertebrate TAU in MBNs result in
506 severe memory deficits without affecting lifespan (Mershin et al., 2004). Thus, our model

507 provides additional evidence that specific populations of MBNs may play a role in lifespan
508 regulation in flies, while reproducing an important, subtle characteristic of FTD.
509 Sequestration of mRNAs is one the mechanisms by which TDP-43 is thought to
510 contribute to neurodegeneration and identifying candidate mRNA targets has helped better
511 understand disease etiology (Bjork et al., 2022; Ramaswami et al., 2013). Although our model is
512 based on TDP-43 overexpression, we note that among the mRNAs enriched with TDP-43 in
513 MBNs we found 12 of 15 physiological targets of TDP-43 previously identified bioinformatically
514 as potential targets of *Drosophila* TDP-43 (*i.e.*, TBPH) based on UG-richness (Langellotti et al.,
515 2018). In future studies, it will be interesting to explore the relationship between splicing and
516 translational targets of TDP-43. Furthermore, the overlap and specificity of some targets for
517 MNs versus MBNs may provide insights into shared mechanisms and neuronal vulnerability in
518 ALS and FTD, respectively.
519 Functional analyses of the mRNAs associated with TDP-43 identify numerous cellular
520 pathways including Wg and Hippo that have been previously implicated in sleep regulation in
521 flies (Harbison et al., 2017). Additionally, our findings of dopamine receptors as candidate
522 mRNA targets is consistent with findings that loss of mesocortical dopaminergic tracts and
523 dopamine receptors in the frontal lobes could contribute to the behavioral symptoms in FTLD
524 (Murley and Rowe, 2018).
525 For functional validation we chose to focus on *dlp*, an mRNA target of TDP-43 that we
526 previously identified in the ALS model of TDP-43 proteinopathy, and a known regulator of
527 Wg/Wnt signaling. Indeed, Wnt signaling is dysregulated in ALS (Chen et al., 2013; Gonzalez-
528 Fernandez et al., 2019), and mRNAs associated with Wg/Wnt pathway are enriched in FTD
529 patient frontal cortices (Santiago et al., 2020), however, this pathway has not yet been broadly
530 implicated in FTD pathophysiology. Using genetic interactions, we found that *dlp* OE in MBNs
531 mitigates TDP-43 dependent working memory deficits, as evidenced by improved alternation in
532 the Y-maze assay. Taken together, these findings support the notion that Wg/Wnt signaling is

533 altered in ALS/FTD and modulating its activity via Dlp mitigates behavioral deficits caused by
534 TDP-43 proteinopathy. In future studies it will be interesting to see how different mRNA targets
535 mitigate specific phenotypic aspects of FTD and identify ALS versus FTD specific targets of
536 TDP-43 proteinopathies.
537

538 **MATERIALS AND METHODS**

539 *Drosophila genetics and maintenance*

540 Flies were maintained at 25°C in 12-hour light-dark cycle with 25-30% humidity. Specific
541 information on *Drosophila* lines used in this study and specific experiments where each line was
542 employed can be found in the Key Resources table (Supplementary information). For aging and
543 lifespan studies, newly eclosed virgin male and female flies were collected and maintained on
544 standard fly cornmeal/molasses media refreshed weekly. Flies harboring *UAS TDP-43::YFP*
545 and *UAS dlp* transgenes for co-overexpression of TDP-43 and Dlp were generated using
546 standard genetic recombination techniques. The presence of *UAS TDP-43::YFP* was confimed
547 by YFP expression when crossed with the pan-neuronal driver, elav GAL4 while Dlp
548 overexpression was confirmed using RT-qPCR (*dlp OE* = 2.45 FC, *TDP-43$^{WT}$::YFP* ; *dlp OE* =
549 3.09 FC, *TDP-43$^{G298S}$::YFP* ; *dlp OE* = 1.71 FC compared to *w$^{1118}$* controls; Figure 6-supplement
550 1B).
551

552 *Western Blotting*

553 1 – 3 day old flies were collected from *SS01276* crossed with 1) *w$^{1118}$; TDP-43$^{WT}$::YFP*, 2) *w$^{1118}$;*
554 *TDP-43$^{WT}$::YFP; dlp OE*, 3) *w$^{1118}$; TDP-43$^{WT}$::YFP mCD8::RFP*, and 4) *w$^{1118}$* in triplicate . Heads
555 (N = 15 for each genotype) were decapitated and homogenized in 100 µl 2X Laemmli Sample
556 Buffer (BIO-RAD 1610737) containing 5% of 2-Mercaptoethanol (Sigma-Aldrich M3148). The
557 homogenized protein samples were boiled for 5 min in the digital Heat Block (Benchmark), and
558 spun for 1 min. Supernatants were collected and 10 µl of protein sample was loaded in each

559 well of precast Mini-PROTEAN TGX 4-20% gradient Gel (BIO-RAD 4561096). Following SDS-
560 PAGE, the proteins were transferred to Nitrocellulose membrane (BIO-RAD 1620215). After
561 transfer, the membrane was blocked in 5% nonfat milk in PBST (PBS and 0.1% TWEEN20) and
562 incubated overnight at 4$^{o}$C with primary antibodies mouse anti-GFP Living Color (Cell Signaling
563 Technology 2955, 1:1000) to detect TDP-43 YFP and rabbit anti-Beta-Actin (Cell Signaling
564 Technology 4967S, 1:1000) as loading control, followed by washes in TBST and incubation with
565 secondary antibody (IRDye® 800CW, Goat anti-Mouse D21115-25, 1:10,000) and
566 (IRDye®680RD Goat anti-Rabbit D21207-05, 1:10,000) for 1 hour at RT. The blot was imaged
567 using a LICOR scanner (Odyssey®DLx) and protein bands intensities were quantified with
568 LICOR "Image Studio Lite" (Figure 7-supplement 2).
569
570 *Statistical analyses*
571 Statistical analyses were conducted in R (v. 4.1.2, R CoreTeam, 2021) and RStudio (v.
572 2021.09.0+351, RStudioTeam, 2022) unless specified otherwise in specific methods. The
573 tidyverse (Wickham et al., 2019) and ggpubr (Kassambara, 2020) packages were used for
574 summary statistics and graphics. Other analysis-specific packages are cited in the
575 corresponding Methods section. While data for the mutant TDP-43$^{G298S}$ model is presented as a
576 supplement to our main findings, statistical analyses were conducted simultaneously for both
577 TDP-43 genotypes and p-values were corrected for multiple comparisons that included both
578 genotypes. For any given analysis when males and females did not differ statistically or sample
579 sizes were low (*e.g.*, histological preparations), they were pooled to increase power. Where
580 necessary, outliers were removed prior to hypothesis testing. When data did not fit the
581 assumptions of parametric models and non-parametric analyses were used, hypothesis testing
582 proceeded by first using a Kruskal-Wallace to test for a difference among groups, followed by
583 pairwise comparisons using the Wilcoxon Rank Sum Test with p-values adjusted for multiple
584 comparisons using the false discovery rate method (Benjamini and Hochberg, 1995). Specific

585 statistical methods are described for each assay. Summary statistics for each figure can be
586 found in the supplemental tables file.
587
588 *Mushroom body morphological analyses*
589 Mushroom body morphology was evaluated using membrane-targeted RFP (mCD8 RFP) driven
590 by *SS01276* (Aso, 2021). Adult brains were dissected in cold HL-3 saline (Stewart et al., 1994),
591 fixed for 60 minutes in 4% paraformaldehyde, then rinsed in phosphate buffered saline (PBS,
592 3X), permeabilized in PBS with 0.25% Triton X-100 (PBST), and blocked in PBST plus 5%
593 normal goat serum (Sigma-Aldrich 566380) 2% bovine serum albumin (Sigma-Aldrich A5611)
594 for 45 minutes prior to antibody labeling. YFP was detected by incubating brains overnight at
595 4°C with a mouse monoclonal anti-GFP FITC antibody (1:300, Rockland 600-302-215). mCD8
596 RFP was visualized using native fluorescence. All brains were mounted on slides with the
597 ventral side containing the mushroom body lobes (MBLs) facing the coverslip. For cell body
598 imaging, brains were additionally incubated in Hoechst (1:10,000, Invitrogen H3570) for 10
599 minutes and mounted on slides with the dorsal side containing the calyx facing the coverslip.
600
601 *Image acquisition and analysis*
602 <u>TDP-43 cytoplasmic localization and MBN cell loss:</u> Images were acquired using a Zeiss 880
603 Laser Scanning Confocal inverted microscope with a Plan-Apochromat 63x/1.4 oil DIC M27
604 lens. TDP-43 YFP signal intensity was quantified per unit area in the nucleus and cell body.
605 Hoechst was used to define the nuclear boundaries, while total cellular TDP-43 signal was
606 measured by tracing a boundary around YFP signal in the entire cell (Figure 1-supplement 3).
607 To quantify the total number of MBNs expressing TDP-43 YFP, all nuclei were counted from
608 optical sections 2 μm apart to ensure nuclei were counted only once. We tested for differences
609 in TDP-43 nuclear to cellular ratio and MBN number by age, sex, and genotype using Analysis
610 of Variance (ANOVA) performed on a linear model (*lm* function in R; R Core Team 2017).

611 Residuals were normally distributed (Shapiro-Wilks test for normality, P = 0.890 and P = 0.395
612 for ratio and MBN number, respectively) and we therefore continued with pairwise comparisons
613 using Tukey's Honest Significant Difference corrected for multiple comparisons.
614 Signal intensity: All images were acquired using a Zeiss 880 Laser Scanning Confocal inverted
615 microscope with a Plan-Apochromat 63x/1.4 oil DIC M27 lens. For mCD8 RFP fluorescence
616 intensity, brains were imaged using either an Alexa Fluor 568 or a DS Red filter set with pinhole
617 adjusted to 1 AU and 3 μm optical section thickness. For measuring anti-GFP FITC
618 fluorescence intensity, brains were imaged using the FITC filter set with the pinhole adjusted to
619 1 AU and 0.5 μm optical section thickness. Fluorescence intensity was measured in FIJI as the
620 integrated density over the sample area in axons by manually tracing α/β or γ lobes and
621 subtracting adjacent background signal. First, a polygon was traced free-hand over the visible
622 area of each lobe (α/β or γ). This polygon was then dragged to an adjacent area of the brain to
623 obtain a mean fluorescence intensity for the background in each section. In instances where the
624 polygon was shaped in such a way that it could not be dragged to adjacent brain area, a
625 comparably-sized polygon was drawn in the adjacent brain region. Intensity was measured in at
626 least three sections to obtain mean fluorescence intensity in each channel (RFP or FITC) for
627 both α/β and γ lobes of each brain. To test for differences in signal intensity within a genotype
628 across age time points, values of signal intensity were normalized to mean signal intensity of
629 young (1- 3 day old) brains of the same genotype and lobe. Statistical analysis of change in
630 fluorescence intensity with age was performed by comparing middle aged (~30 days) or old
631 (~60 days) flies and young (~1 day) flies from the same genotype using the Wilcoxon Rank Sum
632 test. Summary statistics can be found in Supplemental table S2A.
633 YFP particle size: The Analyze Particles function in FIJI was used to identify YFP puncta in MB
634 lobes. Images were first contrast enhanced using a brightness/contrast enhancement (saturated
635 pixels set to 0.3% and normalized) followed by thresholding using the Bernsen method in the

636 Auto Local Threshold function with a 25 – 50 pixel radius depending on image quality. Particles
637 were considered puncta when they were 0.25 – 3.0 $\mu m^2$ in size and showed 0.25 - 1.0
638 circularity. To measure mean particle size in each sample, a polygon was drawn over the visible
639 portion of each lobe in at least three sections for each lobe. From these subsamples we
640 calculated a mean particle size for each lobe of each brain. Summary statistics can be found in
641 Supplemental table S2B.
642 GAL4 dilution effect: To test whether UAS-driven expression of a second transgene reduces
643 UAS-driven TDP-$43^{WT}$ expression, in addition to western blots, we also measured mean pixel
644 intensity from maximum intensity projections of the horizontal lobes ($\beta$ and $\gamma$ combined in
645 maximum intensity projection) in two genotypes with *SS01276*-driven transgenes, *OR-R ;TDP-*
646 *$43^{WT}$::YFP* and *$w^{1118}$ ; TDP-$43^{WT}$::YFP mCD8::RFP* (Figure 7-supplement 3).
647
648 *Behavioral assays*
649 Y-maze: To measure changes in working memory, we employed a y-maze assay described by
650 Lewis et al. (2017). We tracked the two-dimensional movement of individual *Drosophila* placed
651 in small symmetrical Y-mazes using video recordings for ten 1-minute trials following two
652 minutes of acclimation time in the maze. Observations took place between 08:45 and 11:00 and
653 14:00 to 16:00 when flies were most active. Male and female flies were run separately and the
654 locations of genotypes in the 7 by 7 maze array were randomized for each set of trials. Assays
655 were conducted in a dark room with each maze lit uniformly from below with a white LED array
656 and capped with a clear Plexiglas coverslip. The overall movement of flies and visits to three
657 unique arms consecutively were quantified using the Noldus Ethovision software. Spontaneous
658 alternation behavior was measured by scoring three consecutive arm entries in a sliding window
659 for each of ten trials. The alternation score was calculated as alternations divided by alternation
660 attempts. Movement and alternation data were summed for each fly during each 1-minute trial

661 and then averaged over ten trials for statistical analyses. Flies originating from three biological
662 replicates were pooled for analysis (Supplementary table S3). The large samples sizes
663 permitted the use of parametric tests, and we assessed differences in distance moved or
664 alternation score across genotypes using ANOVA on a linear mixed-effects model (lmer function
665 in R; Bates et al., 2015) that included replicate as a fixed effect. Flies that performed no
666 alternations naturally did not have a percent alternation score and were removed from
667 subsequent analysis. Males and females were analyzed separately. Flies were additionally
668 assessed for the presence of bias for specific arms, calculated as a ratio of the mean number of
669 entries into each arm over mean total entries and tested for significant variation from 0.333
670 using the Wilcoxon Signed Rank test. Interestingly, while females showed no arm biases, males
671 overexpressing *TDP-43*$^{WT}$ and OR-R controls showed a bias against arm B (*TDP-43*$^{WT}$, $\bar{x}$ =
672 0.307 ± 0.08, P < 0.0001; OR-R, $\bar{x}$ = 0.316 ± 0.13, P = 0.0038). *TDP-43*$^{WT}$ also showed a bias
673 for arm A ($\bar{x}$ = 0.352 ± 0.076, P = 0.0033), while OR-R controls showed a bias for arm C ($\bar{x}$ =
674 0.347 ± 0.113, P = 0.048). Although these analyses suggest that arm biases exist in males and
675 are not unique to TDP-43 overexpression, a single replicate was used to test whether Dlp
676 overexpression could rescue alternation deficits seen in TDP-43 overexpressing flies therefore
677 hypothesis testing proceeded with non-parametric tests as described in *Statistical analyses*.
678 Sleep: Adult flies from the three age time points were monitored individually using *Drosophila*
679 Activity Monitors (DAMs; Trikinetics, Waltham, MA; Chiu et al., 2010). Flies were placed in
680 monitoring tubes with a small amount of food the day before they reached 2-3, 31-33, or 61-63
681 days old. Sleep and activity monitoring began at 12 AM following placement of flies in the sleep
682 incubator, allowing flies at least six hours prior to the start of the experiment to acclimate to the
683 tubes. Sleep and locomotor activity data were collected at 1-minute intervals for three days and
684 analyzed using ShinyR-DAM (Cichewicz and Hirsh, 2018). In *Drosophila ,* sleep is defined at 5
685 minutes of inactivity (Shaw et al., 2000) and here sleep data were processed using the ShinyR
686 DAM program (Cichewicz and Hirsh 2018), which provided average sleep, sleep bout number

687 and duration, and activity to sleep bout length ratio. Comparison of these variables by age and
688 genotype were conducted separately for male and female flies. Data from two replicates were
689 pooled (> 15 flies per genotype x replicate; sample sizes in supplemental tables S4A, S4B).
690
691 *Lifespan*
692 Newly eclosed virgin males and females were separated and placed on fresh food, then
693 transferred weekly into new food vials. The number of surviving flies was counted every other
694 day for 100 days. Survival analysis and plots were generated using R packages *survival*
695 (Therneau, 2021) and *survivminer* (Kassambara et al., 2021).
696
697 *mRNA targets of TDP-43*
698 RNA Immunoprecipitations: Equal numbers of male and female flies, aged 1-3 days, were
699 pooled in Eppendorf tubes and flash frozen in liquid nitrogen. A minimum of 500 flies expressing
700 YFP, TDP-43$^{WT}$ YFP, or TDP-43$^{G298S}$ YFP were collected for each of three biological replicates.
701 Frozen flies were then transferred to 50mL conical tubes and heads were separated from the
702 bodies using four rounds of vortexing and flash freezing with liquid nitrogen. A sieve was used
703 to filter out the bodies and isolated heads were collected into tubes containing lysis beads (Next
704 Advance Green lysis beads). Heads were homogenized (Next Advance Bullet Blender) in 1mL
705 fresh lysis buffer (DEPC water, 50 mM HEPES buffer pH 7.4, 0.5% Triton X-100, 150 mM NaCl,
706 30 mM EDTA), protease inhibitors (cOmplete™, Mini, EDTA-free Protease Inhibitor Cocktail,
707 Millipore Sigma 11873580001), and RNAsin Plus 400 u/mL (Fischer Scientific PRN2615),
708 centrifuged for 10 minutes at 10,000 rpm, and the lysate was collected. A portion of the lysate
709 was saved for the protein input and RNA input samples. For protein input, the lysate was mixed
710 with 2X Laemmli buffer, boiled at 95-100$^{o}$C for 10 minutes, and stored at -20$^{o}$C. For RNA input,
711 TRIzol reagent (Thermofisher 15596026) was added to the lysate and the sample was stored at
712 -80$^{o}$C. High affinity GFP-Trap magnetic agarose beads (ChromoTek) were added to the

713 remaining lysate and rotated end-over-end for 90 minutes at 4$^{o}$C to allow for binding of YFP.
714 The beads were separated from the lysate with a magnet and washed three times with fresh
715 wash buffer (DEPC water, 50 mM HEPES buffer pH 7.4, 0.5% Triton X-100, 150 mM NaCl, 30
716 mM EDTA). The beads were resuspended in wash buffer and split into two tubes for the protein
717 IP and RNA IP samples. For the protein IP sample, 2X Laemmli buffer was added to the beads,
718 samples were boiled at 95-100$^{o}$C for 10 minutes, and the beads were removed with a magnet.
719 Western blots (see above) were performed to ensure that the immunoprecipitated complexes
720 contained TDP-43 before processing the RNA IPs. For the RNA IP sample, TRIzol reagent was
721 added to the beads, the solution was pipetted up and down for 60 seconds, and the beads were
722 removed with a magnet.
723 RNA-Seq: RNA was quantified by nanodrop to bring it within range for ribogreen quantification.
724 RNA was also checked using Agilent Tapestation High Sensitivitiy RNA screentape. 1 ng total
725 RNA was used for SMART-Seq HT PLUS (Takara Bio USA, Inc. Cat # R400748) following
726 manufacturer's protocol. Determination of cDNA quality and quantity was determined via Agilent
727 Tapestation High Sensitivity D5000 Screentape and Qubit dsDNA HS assay for input into library
728 amplification. Libraries were quantified by Agilent Tapestation High Sensitivity D1000
729 Screentape and Kapa Library Quantification kit for Illumina platforms. Libraries were pooled
730 equimolarly, pools were quantified by Agilent Tapestation High Sensitivity D1000 Screentape
731 and Kapa Library Quantification kit and loaded on the NovaSeq 6000 S4 flowcell and
732 sequenced to 101 x 11 x 11 x 101 cycles. Trimmed fastqs were aligned to the Dmel genome
733 with STAR v2.6.1d (Dobin et al., 2013). Aligned reads were counted with featureCounts v1.6.3
734 (Liao et al., 2014) using the genome annotation. Files produced for individual samples were
735 aggregated into a single .txt file using python. Differential expression was quantified using
736 DESeq2 (Love et al., 2014). We included overexpression of cytoplasmic YFP in MBNs as a
737 control for IPs, however the expression levels of YFP alone were far greater than cytoplasmic
738 TDP-43 YFP (data not shown), making it difficult to assess the role of cytoplasmic YFP alone.

739 To ensure that candidate mRNA targets showing the greatest enrichment were indeed specific
740 in their association with TDP-43, we subtracted YFP control Log2FC values from the Log2FC
741 values of targets recovered in each of our models. Indeed, in this YFP-subtracted analysis
742 *futsch* was recovered as enriched with TDP-43 in both variants (Figure 6A, Figure 6-figure
743 supplement 1A) and the majority of mRNAs that showed high enrichment in the original analysis
744 were retained in the YFP-subtracted analyses (Figure 6A vs 6D, Supplemental figure S6A vs
745 S6C).
746 Functional annotation: The Database for Annotation, Visualization, and Integrated Discovery
747 (DAVID) was used to functionally annotated genes enriched with TDP-43 (Dennis et al., 2003;
748 Sherman et al., 2022). To assess genes over-represented in our disease model data sets, we
749 used lists of genes significantly enriched with each of our TDP-43 models (differential gene
750 expression lists available in source data).
751 RNA Extraction for Validation: RNA input and RNA IP samples, stored in TRIzol reagent
752 (Thermofisher 15596026) at -80$^{o}$C, were allowed to thaw completely on ice and chloroform was
753 added to each sample. Samples were shaken briefly to mix, left to incubate for 3 minutes at
754 room temperature, and then centrifuged at 12,000 rpm for 15 minutes at 4$^{o}$C to allow for
755 separation of the aqueous and organic phases. The RNA-containing aqueous phase was
756 collected and molecular grade isopropyl alcohol was added to each sample. Samples were
757 incubated for 10 minutes at room temperature for RNA precipitation and then centrifuged at
758 12,000 rpm for 10 minutes. The pelleted RNA was washed with 75% ethanol (200 proof ethanol
759 & HyPure water) and left to dry in a fume hood. RNA was resuspended in HyPure water and the
760 concentration and 260/280 absorbance ratio were measured using Nanodrop.
761 RT-qPCR: RNA extracted from input and IP samples was used as template RNA for cDNA
762 synthesis by reverse transcription. Total RNA used in the cDNA synthesis reactions was
763 normalized across samples. cDNA was synthesized using the Fisher First Strand cDNA
764 synthesis kit (Thermofisher Scientific K1641). qPCR reactions were prepared in a 96-well qPCR

765 plate, in triplicates, using Taqman Fast Advanced Master Mix (Thermofisher Scientific 4444556)
766 and Taqman probes for Dally-like protein (dlp) (Thermofisher Scientific Dm01798597_m1) and
767 Gpdh1 (Thermofisher Scientific Dm01841185_m1). qPCR was conducted on the qTOWER
768 (Analytik Jena 844-00504-4) qPCR machine. Delta Ct was calculated as the difference in Ct
769 values (dlp - gpdh1). To determine enrichment of dlp mRNA in the IPs, ΔΔCt was calculated as
770 the difference in Delta Ct values (IP - Input). Fold change was calculated as 2^(-ΔΔCt).
771 Dally-like protein target validation: Brains from flies 1-3 days or 50-55 days were dissected out
772 and the tissue fixed, permeabilized and blocked as described above. Brains were then
773 incubated overnight at 4°C in an anti-Dally-like protein antibody at 1:5 in block (13G8 developed
774 by Phil Beachy, obtained from the Developmental Studies Hybridoma Bank, created by the
775 NICHD of the NIH and maintained at The University of Iowa, Department of Biology, Iowa City,
776 IA 52242, targets amino acids V523 to Q702), rinsed 3X in 0.1% PBST and incubated in goat
777 anti-mouse Alexa Flour 647 antibody overnight at 4°C (1:300, ThermoFisher A32728). Images
778 were acquired using a Zeiss 880 Laser Scanning Confocal inverted microscope with a Plan-
779 Apochromat 63x/1.4 oil DIC M27 lens. Signal intensity was traced from maximum intensity
780 projections of the MBLs and normalized to background intensity. Dlp signal intensity declined
781 with age in TDP-43 flies, so the mCD8-RFP channel was used to trace the lobes in aged brains,
782 ensuring the correct lobe area was used for signal intensity measurements.

783 **DATA AVAILABILITY**

784 Summary statistics for each figure can be found in the supplemental tables file. Source data are
785 available from ScholarSphere (doi:10.26207/jq6p-w169) and are cataloged in the Key
786 Resources table. Please refer to the included readme file for variable descriptions. RNA-seq
787 data are available from NCBI GEO Bioproject GSE217213.

788

789 **ACKNOWLEDGEMENTS**

790 We would like to thank Patty Jansma at the University of Arizona Imaging Cores - Optical
791 Facility for her consultation on sample preparation and image acquisition and Dr. Shaun Davis
792 in the Schlenke lab at UArizona for generating TDP-43 transgenic lines in a OR-R background.
793 We thank Erik Lehmkuhl for his advice on immunoprecipitation experiments and interpretation of
794 RNA-seq data. We also acknowledge Dr. Robert Kraft for generating UAS TDP-43 UAS mCD8
795 RFP recombinant stocks. We thank Dr. Yoshi Aso (HHMI) for sharing the *SS01276* GAL4 line
796 and Dr. Fabian Fernandez (UArizona) for Y-maze training. Support for Hillary Cowell Ruvalcaba
797 was provided in part by The University of Arizona's Undergraduate Research Opportunities
798 Consortium Prep (UROC-Prep) Program. The University of Arizona Maximizing Access to
799 Research Careers (MARC Training Grant NIGMS T34 GM008718) program provided support
800 for Grace Hala'ufia. We would like to acknowledge members of the Zarnescu lab for their advice
801 on experimental design and data analysis, and feedback on the manuscript.

802 Figures

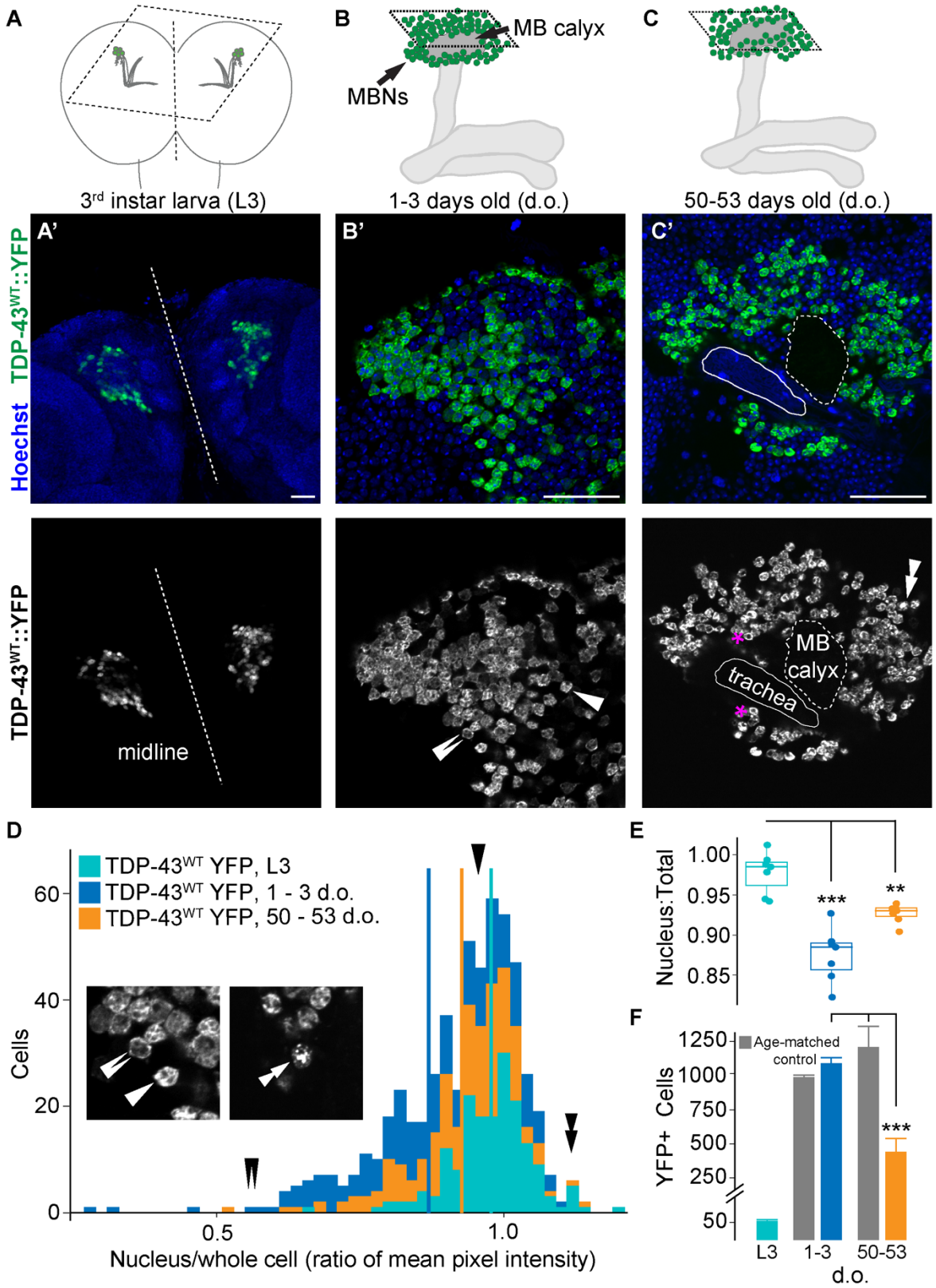


803

804 Figure 1. *TDP-43$^{WT}$* overexpression in Kenyon Cells results in cytoplasmic mis-localization and
805 age-dependent cell loss. Illustrations in (A), (B), and (C) correspond to approximate plane of
806 imaging for Kenyon cells in (A') larval, (B') young adult, and (C') old adult brain. (A') Nuclear
807 localization of human TDP-43$^{WT}$ YFP in the larval MBNs. (B') Young adult flies (1 – 3 days)
808 contain cells with TDP-43$^{WT}$ YFP in the cell body and cells showing nuclear loss of TDP-43$^{WT}$
809 YFP (adjacent, double arrows as compared with single arrow). (C') Old adults (50 – 55 days)
810 have fewer cells with nuclear depletion but concurrent loss in total number of TDP-43$^{WT}$ positive
811 neurons (quantified in E and F). Stacked, double arrows indicate a cell that has a signal
812 intensity ratio > 1.0 due to punctate TDP-43 signal in the nucleus. Magenta asterisks indicate
813 cells where nuclear depletion can be detected visually. (D) Histograms showing distribution of
814 TDP-43$^{WT}$ YFP signal intensity ratios (cell nuclei to total cell) shift with age. Arrows correspond
815 to measurements taken from cells shown in figure inset taken from (B'), (C'). (E) Age-specific
816 TDP-43$^{WT}$ YFP signal intensity ratios. (F) Decrease in TDP-43$^{WT}$ YFP positive cells from young
817 to old adults. *SS01276 > YFP* used as age-matched controls. Larval cell numbers provided for
818 reference, but not used in statistical comparisons. Data for TDP-43$^{G298S}$ YFP presented in
819 Figure 1-supplement 2. Scale bars = 50 μm. ** = P < 0.01; *** = P < 0.001.

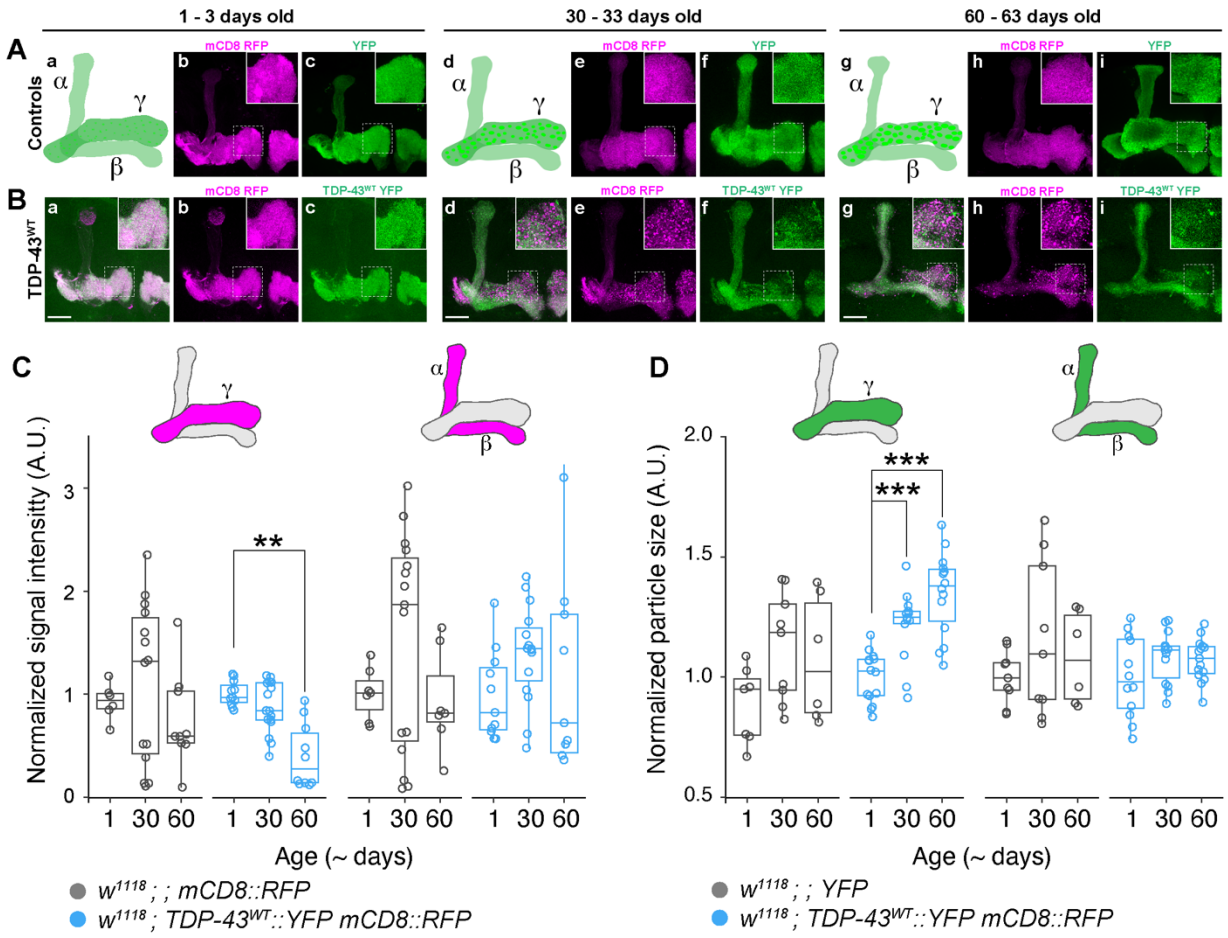


Figure 2. Mushroom body lobes (MBLs) show age-related, region-specific *TDP-43$^{WT}$* accumulation and axonal fragmentation. (A) Illustrations of MBLs targeted by *TDP-43$^{WT}$* OE and observed changes with age (a, intact in young flies; d, increasingly punctate TDP-43 YFP by middle-age; g, axonal thinning and evidence of degeneration specifically in the γ lobe). These are presented alongside morphology of young (b, c,) middle-aged (e, f) and old (h, i) control flies expressing membrane-bound RFP (mCD8 RFP) or cytoplasmic YFP. (B) Overexpression of TDP-43$^{WT}$ YFP in MBNs results in axonal localization of TDP-43 in young adult flies (c) and dystrophic neurites in middle-aged (e) and old (h) flies. (C) Signal intensity of mCD8 RFP with age in γ (left) and α/β (right) lobes. (D) Changes in TDP-43$^{WT}$ YFP particle size with age in γ (left) and α/β (right) lobes. Data for TDP-43$^{G298S}$ presented in Figure 2-supplement 1. Scale bar = 25 μm * = P <0.05; ** = P < 0.01; *** = P < 0.001.

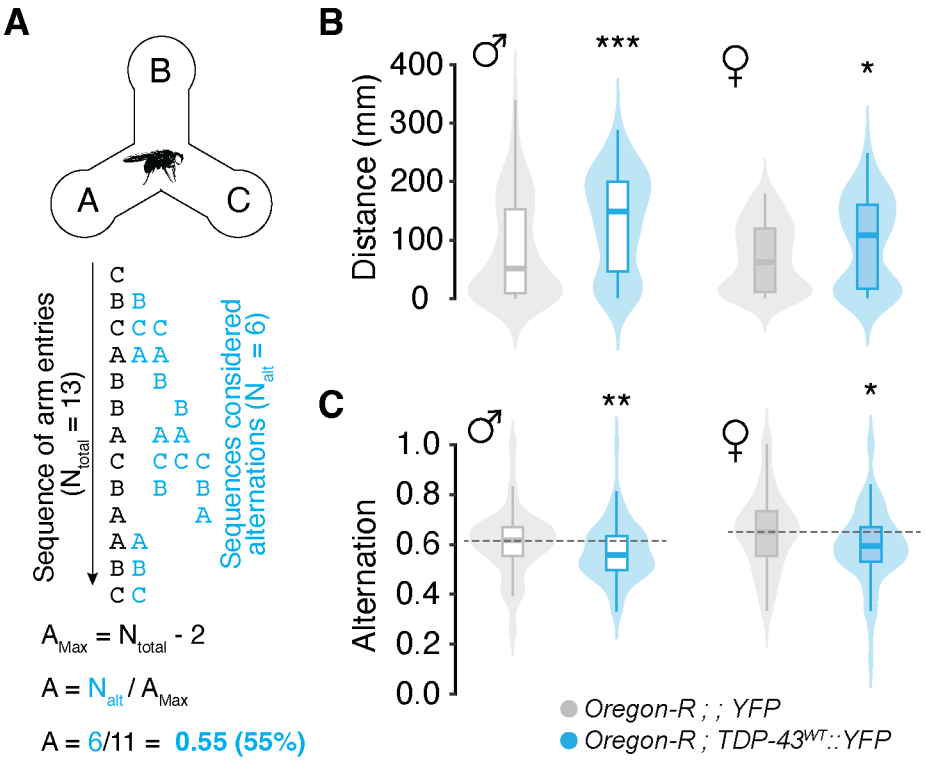


Figure 3. Overexpression of TDP-43 in mushroom body MBNs results in spatial working memory deficits. (A) Schematic of the spatial working memory assay showing the sequence of decisions made by a fly (black text) and those coded as alternations (blue text). Alternation scores were calculated as the number of alternations ($N_{alt}$) divided by alternation attempts ($A_{max}$). (B) Young (1-3 days old) flies with TDP-43$^{WT}$ YFP OE show significant increases in movement. (C) Despite moving more, these flies show reduced alternation percent when compared with controls. Grey dotted line = control group median. A% = alternation percent. * = P <0.05; ** = P < 0.01; *** = P < 0.001.

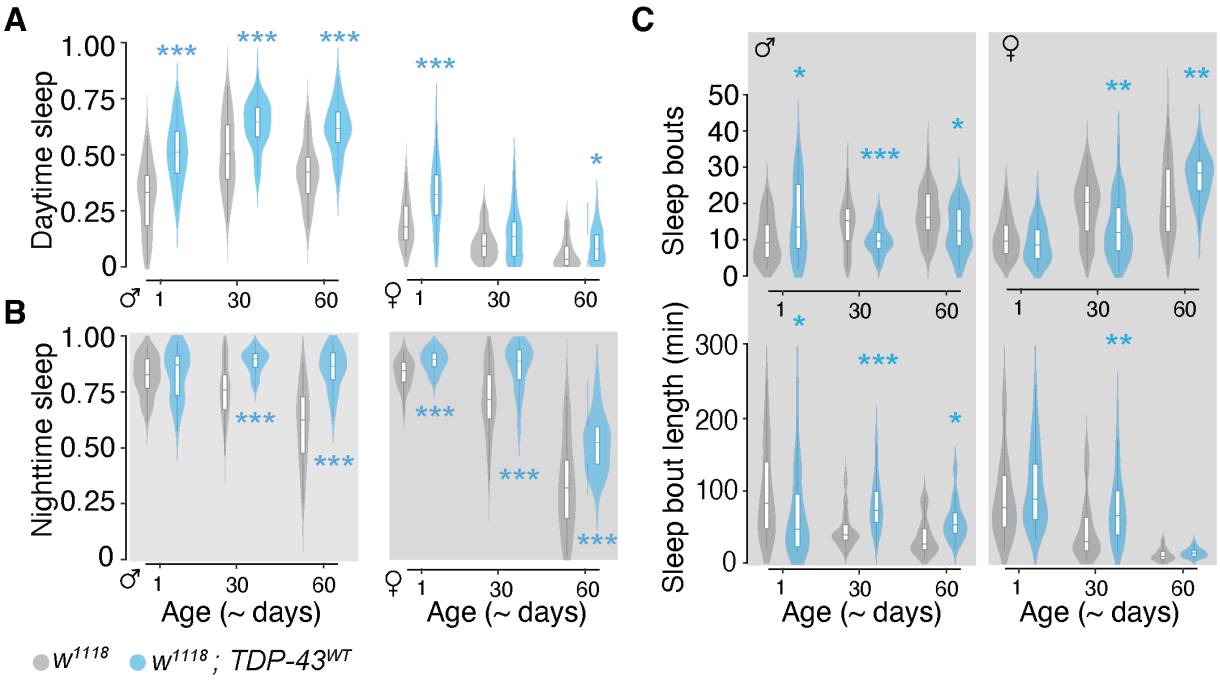


Figure 4. TDP-43$^{WT}$ overexpression in mushroom body MBNs reduces arousal, increasing day and night sleep. (A) Proportion of time flies spent sleeping during the day and (B) at night. (C) Sleep fragmentation assessed by number of sleep bouts (top panel) and mean bout length (bottom panel) during the night. Male data on the left and female data on the right in each panel. Data for TDP-43$^{G298S}$ presented in Figure 4-supplement 1. * = P <0.05; ** = P < 0.01; *** = P < 0.001

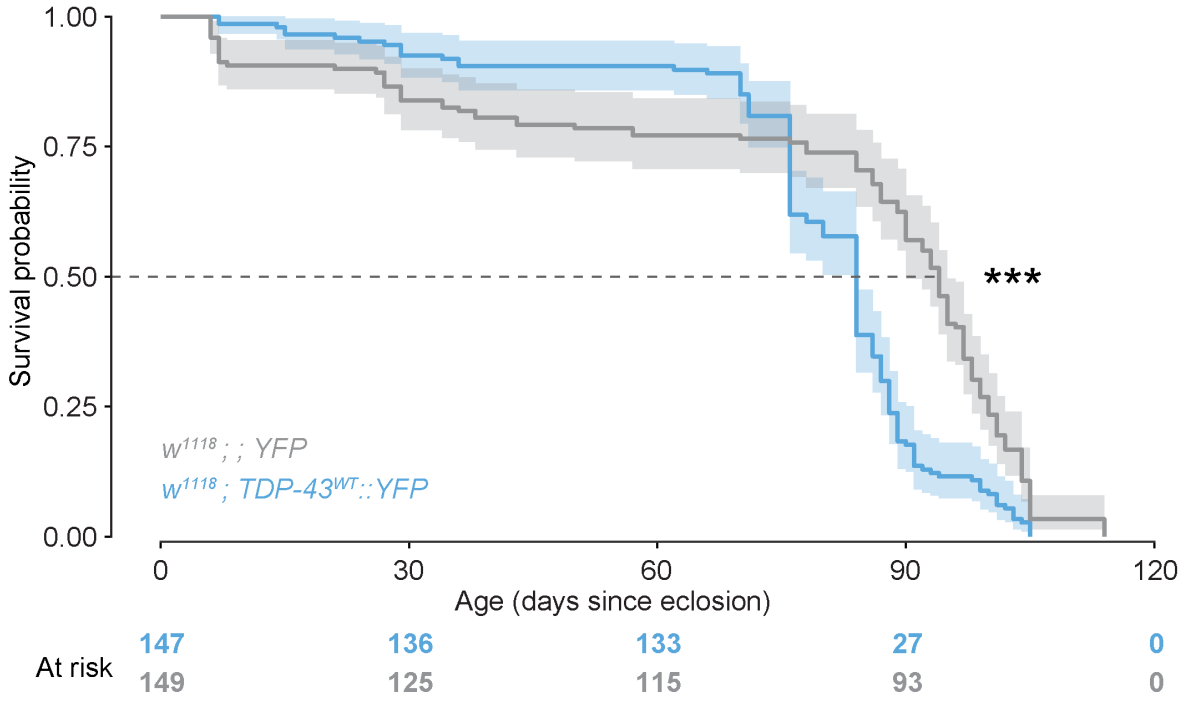


850

851 Figure 5. TDP-43 overexpression in MBs is sufficient to reduce lifespan. Data from male and

852 female flies pooled for analysis. Number of flies N=149 for YFP controls and 147 for TDP-43$^{WT}$

853 YFP expressing flies). Data for TDP-43$^{G298S}$ presented in Figure 5-supplement 1. *** $P < 0.001$

854

855

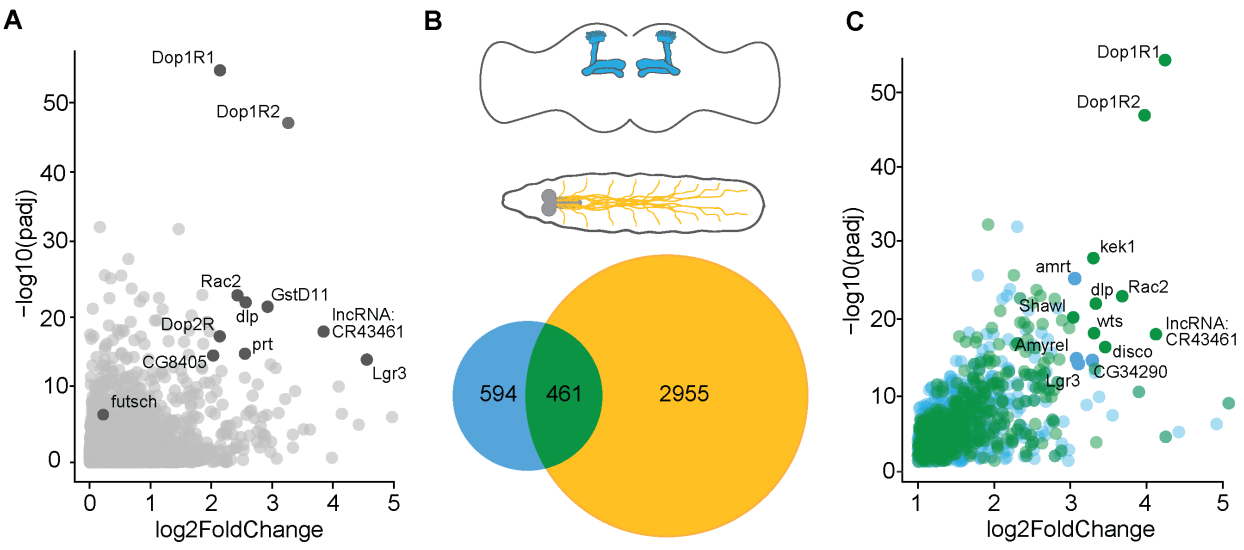


Figure 6. mRNAs enriched with TDP-43 in *Drosophila* models of proteinopathy in FTD and ALS. (A) Volcano plot displaying mRNAs enriched with TDP-43. Y-axis depicts Log2 Fold Change after subtraction of YFP control values (see Materials and Methods). A small number of targets showing greatest enrichment with high confidence are highlighted with blue circles (log2 Fold Change > 2 and $P < 1 \times 10^{-14}$). (B) Schematic showing subsets of neurons in fly models of FTD (MBs, above) and ALS (MNs, below), and Venn diagram depicting enriched mRNAs unique to MB and MN circuits, and overlapping between models. (C) Volcano plot displaying mRNAs enriched in TDP-43 complexes that are MB-specific (blue) or shared between MB and MN models (green); saturated green circles indicate shared targets that show log2 Fold Change > 3 and $P < 1 \times 10^{-14}$; blue circles indicate MB targets with log2 Fold Change > 2 and $P < 1 \times 10^{-14}$. Data for TDP-43$^{G298S}$ presented in Figure 6-supplement 1.

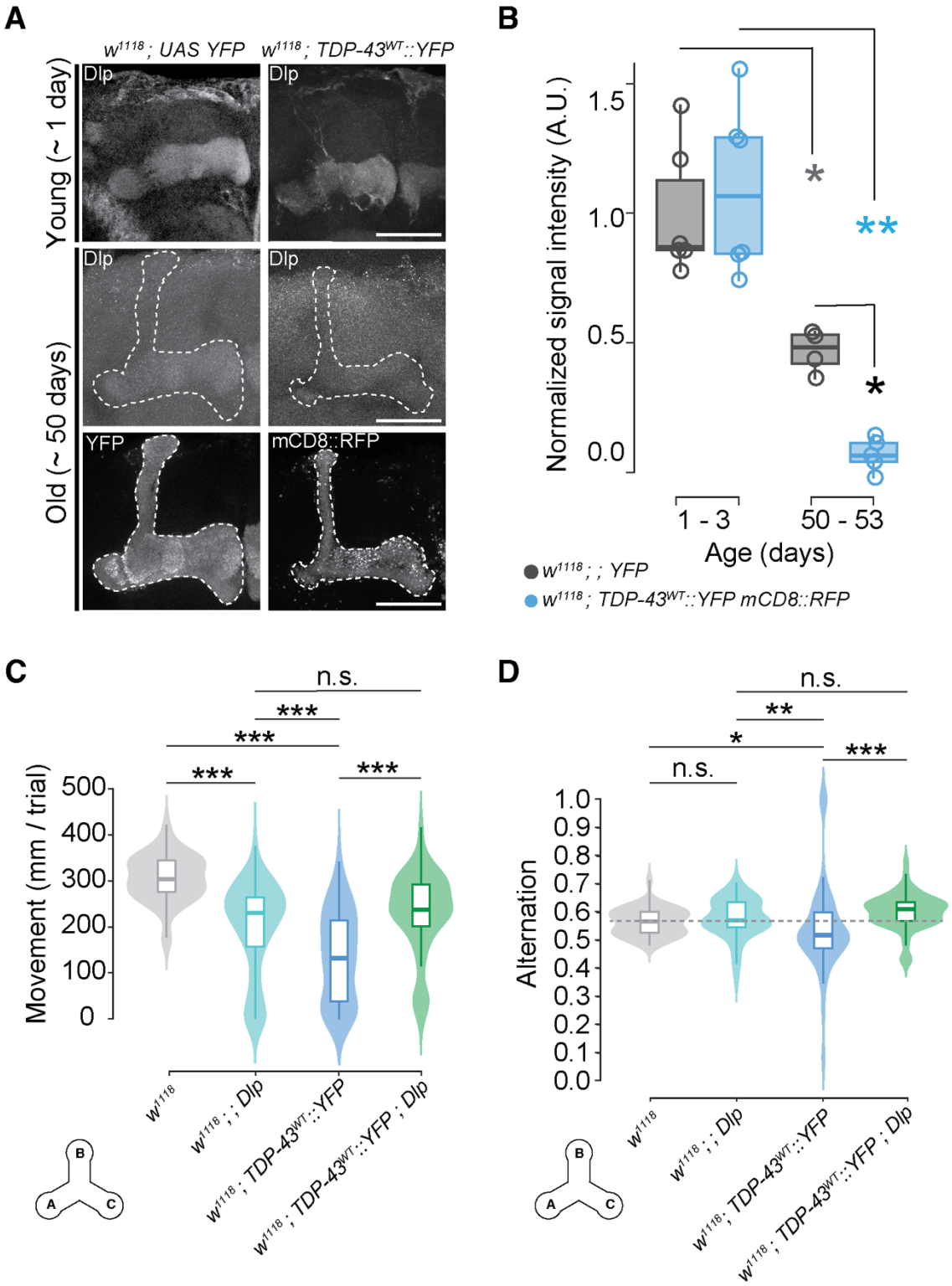
A
w1118 ; UAS YFP
w1118 ; TDP-43WT::YFP
Young (~ 1 day)
Old (~ 50 days)
Dlp
YFP
mCD8::RFP
B
Normalized signal intensity (A.U.)
1.5
1.0
0.5
0.0
1 - 3
50 - 53
Age (days)
w1118 ; ; YFP
w1118 ; TDP-43WT::YFP mCD8::RFP
C
Movement (mm / trial)
500
400
300
200
100
0
n.s.
***
w1118
w1118 ; ; Dlp
w1118 ; TDP-43WT::YFP
w1118 ; TDP-43WT::YFP ; Dlp
D
Alternation
1.0
0.9
0.8
0.7
0.6
0.5
0.4
0.3
0.2
0.1
0.0
n.s.
*
**
***

871 Figure 7. Dally-like protein is a target of TDP-43$^{WT}$ in MBNs where it mediates TDP-43
872 dependent working memory deficits. (A) Dlp antibody labelling in mushroom bodies shows age
873 and TDP-43 dependent reduction. Genotypes (*$w^{1118}$; YFP* and *$w^{1118}$; TDP-43$^{WT}$::YFP*
874 *mCD8::RFP*), stainings (Dlp, YFP, RFP) and ages (1 and ~ 50 days old), as indicated. (B)
875 Quantification of age and TDP-43 dependent changes in Dlp signal intensity within MBLs. (C)
876 Mean distance moved and (D) alternation per trial in males overexpressing Dlp (*$w^{1118}$ ; ; dlp*
877 *OE),* TDP-43$^{WT}$ (*$w^{1118}$ ; TDP-43$^{WT}$::YFP)* or both *($w^{1118}$ ; TDP-43$^{WT}$::YFP; dlp OE*) compared to
878 *$w^{1118}$* genetic background controls. Grey dotted line represents control group median. Scale bar
879 = 50 μm. Data for TDP-43$^{G298S}$ presented in Figure 7-supplement 1. * = P < 0.05, ** = P < 0.01

880 **REFERENCES**


881 Al-Chalabi, A., Jones, A., Troakes, C., King, A., Al-Sarraj, S., and van den Berg, L.H. (2012).
882 The genetics and neuropathology of amyotrophic lateral sclerosis. Acta Neuropathol *124*, 339-
883 352. 10.1007/s00401-012-1022-4.

884 Alami, N.H., Smith, R.B., Carrasco, M.A., Williams, L.A., Winborn, C.S., Han, S.S., Kiskinis, E.,
885 Winborn, B., Freibaum, B.D., Kanagaraj, A., et al. (2014). Axonal transport of TDP-43 mRNA
886 granules is impaired by ALS-causing mutations. Neuron *81*, 536-543.
887 10.1016/j.neuron.2013.12.018.

888 Altman, T., Ionescu, A., Ibraheem, A., Priesmann, D., Gradus-Pery, T., Farberov, L., Alexandra,
889 G., Shelestovich, N., Dafinca, R., Shomron, N., et al. (2021). Axonal TDP-43 condensates drive
890 neuromuscular junction disruption through inhibition of local synthesis of nuclear encoded
891 mitochondrial proteins. Nat Commun *12*, 6914. 10.1038/s41467-021-27221-8.

892 Amador-Ortiz, C., Lin, W.L., Ahmed, Z., Personett, D., Davies, P., Duara, R., Graff-Radford,
893 N.R., Hutton, M.L., and Dickson, D.W. (2007). TDP-43 immunoreactivity in hippocampal
894 sclerosis and Alzheimer's disease. Ann Neurol *61*, 435-445. 10.1002/ana.21154.

895 Arai, T., Hasegawa, M., Akiyama, H., Ikeda, K., Nonaka, T., Mori, H., Mann, D., Tsuchiya, K.,
896 Yoshida, M., Hashizume, Y., and Oda, T. (2006). TDP-43 is a component of ubiquitin-positive
897 tau-negative inclusions in frontotemporal lobar degeneration and amyotrophic lateral sclerosis.
898 Biochem Biophys Res Commun *351*, 602-611. 10.1016/j.bbrc.2006.10.093.

899 Ash, P.E., Zhang, Y.J., Roberts, C.M., Saldi, T., Hutter, H., Buratti, E., Petrucelli, L., and Link,
900 C.D. (2010). Neurotoxic effects of TDP-43 overexpression in C. elegans. Hum Mol Genet *19*,
901 3206-3218. 10.1093/hmg/ddq230.

902 Aso, Y. (2021). Split-GAL4 Mushroom Body Driver Line

903 Aso, Y., Grubel, K., Busch, S., Friedrich, A.B., Siwanowicz, I., and Tanimoto, H. (2009). The
904 mushroom body of adult Drosophila characterized by GAL4 drivers. J Neurogenet *23*, 156-172.
905 10.1080/01677060802471718.

906 Aso, Y., Hattori, D., Yu, Y., Johnston, R.M., Iyer, N.A., Ngo, T.T., Dionne, H., Abbott, L.F., Axel,
907 R., Tanimoto, H., and Rubin, G.M. (2014). The neuronal architecture of the mushroom body
908 provides a logic for associative learning. Elife *3*, e04577. 10.7554/eLife.04577.

909 Ayala, Y.M., Pantano, S., D'Ambrogio, A., Buratti, E., Brindisi, A., Marchetti, C., Romano, M.,
910 and Baralle, F.E. (2005). Human, Drosophila, and C.elegans TDP43: nucleic acid binding
911 properties and splicing regulatory function. J Mol Biol *348*, 575-588. 10.1016/j.jmb.2005.02.038.

912 Azpurua, J., El-Karim, E.G., Tranquille, M., and Dubnau, J. (2021). A behavioral screen for
913 mediators of age-dependent TDP-43 neurodegeneration identifies SF2/SRSF1 among a group

914 of potent suppressors in both neurons and glia. PLoS Genet *17*, e1009882.
915 10.1371/journal.pgen.1009882.

916 Baier, A., Wittek, B., and Brembs, B. (2002). Drosophila as a new model organism for the
917 neurobiology of aggression? J Exp Biol *205*, 1233-1240. 10.1242/jeb.205.9.1233.

918 Bates, D., Mächler, M., Bolker, B., and Walker, S. (2015). Fitting Linear Mixed-Effects Models
919 Usinglme4. Journal of Statistical Software *67*. 10.18637/jss.v067.i01.

920 Bellen, H.J. (1998). The fruit fly: a model organism to study the genetics of alcohol abuse and
921 addiction? Cell *93*, 909-912. 10.1016/s0092-8674(00)81195-2.

922 Benjamini, Y., and Hochberg, Y. (1995). Controlling the False Discovery Rate A Practical and
923 Powerful Approach to Multiple Testing. Journal of the Royal Statistical Society. Series B
924 (Methodological) *57*, 289-300.

925 Bier, E. (2005). Drosophila, the golden bug, emerges as a tool for human genetics. Nat Rev
926 Genet *6*, 9-23. 10.1038/nrg1503.

927 Bjork, R.T., Mortimore, N.P., Loganathan, S., and Zarnescu, D.C. (2022). Dysregulation of
928 Translation in TDP-43 Proteinopathies: Deficits in the RNA Supply Chain and Local Protein
929 Production. Front Neurosci *16*, 840357. 10.3389/fnins.2022.840357.

930 Bonakis, A., Economou, N.T., Paparrigopoulos, T., Bonanni, E., Maestri, M., Carnicelli, L., Di
931 Coscio, E., Ktonas, P., Vagiakis, E., Theodoropoulos, P., and Papageorgiou, S.G. (2014). Sleep
932 in frontotemporal dementia is equally or possibly more disrupted, and at an earlier stage, when
933 compared to sleep in Alzheimer's disease. J Alzheimers Dis *38*, 85-91. 10.3233/JAD-122014.

934 Borroni, B., Bonvicini, C., Alberici, A., Buratti, E., Agosti, C., Archetti, S., Papetti, A., Stuani, C.,
935 Di Luca, M., Gennarelli, M., and Padovani, A. (2009). Mutation within TARDBP leads to
936 Frontotemporal Dementia without motor neuron disease. Human Mutation *30*, E974-E983.
937 10.1002/humu.21100.

938 Bridi, J.C., Ludlow, Z.N., Kottler, B., Hartmann, B., Vanden Broeck, L., Dearlove, J., Goker, M.,
939 Strausfeld, N.J., Callaerts, P., and Hirth, F. (2020). Ancestral regulatory mechanisms specify
940 conserved midbrain circuitry in arthropods and vertebrates. Proc Natl Acad Sci U S A *117*,
941 19544-19555. 10.1073/pnas.1918797117.

942 Cairns, N.J., Neumann, M., Bigio, E.H., Holm, I.E., Troost, D., Hatanpaa, K.J., Foong, C., White,
943 C.L., 3rd, Schneider, J.A., Kretzschmar, H.A., et al. (2007). TDP-43 in familial and sporadic
944 frontotemporal lobar degeneration with ubiquitin inclusions. Am J Pathol *171*, 227-240.
945 10.2353/ajpath.2007.070182.

946 Chakraborty, R., Vepuri, V., Mhatre, S.D., Paddock, B.E., Miller, S., Michelson, S.J., Delvadia,
947 R., Desai, A., Vinokur, M., Melicharek, D.J., et al. (2011). Characterization of a Drosophila

948 Alzheimer's disease model: pharmacological rescue of cognitive defects. PLoS One *6*, e20799.
949 10.1371/journal.pone.0020799.

950 Chang, X.-L., Tan, M.-S., Tan, L., and Yu, J.-T. (2015). The Role of TDP-43 in Alzheimer's
951 Disease. Molecular Neurobiology *53*, 3349-3359. 10.1007/s12035-015-9264-5.

952 Chen, H.J., Topp, S.D., Hui, H.S., Zacco, E., Katarya, M., McLoughlin, C., King, A., Smith, B.N.,
953 Troakes, C., Pastore, A., and Shaw, C.E. (2019). RRM adjacent TARDBP mutations disrupt
954 RNA binding and enhance TDP-43 proteinopathy. Brain *142*, 3753-3770.
955 10.1093/brain/awz313.

956 Chen, Y., Guan, Y., Zhang, Z., Liu, H., Wang, S., Yu, L., Wu, X., and Wang, X. (2013). Wnt
957 signaling pathway is involved in the pathogenesis of amyotrophic lateral sclerosis in adult
958 transgenic mice. Neurological Research *34*, 390-399. 10.1179/1743132812y.0000000027.

959 Chiu, J.C., Low, K.H., Pike, D.H., Yildirim, E., and Edery, I. (2010). Assaying locomotor activity
960 to study circadian rhythms and sleep parameters in Drosophila. J Vis Exp. 10.3791/2157.

961 Chou, C.-C., Zhang, Y., Umoh, M.E., Vaughan, S.W., Lorenzini, I., Liu, F., Sayegh, M., Donlin-
962 Asp, P.G., Chen, Y.H., Duong, D.M., et al. (2018). TDP-43 pathology disrupts nuclear pore
963 complexes and nucleocytoplasmic transport in ALS/FTD. Nature Neuroscience *21*, 228-239.
964 10.1038/s41593-017-0047-3.

965 Cichewicz, K., and Hirsh, J. (2018). ShinyR-DAM: a program analyzing Drosophila activity,
966 sleep and circadian rhythms. Commun Biol *1*, 25. 10.1038/s42003-018-0031-9.

967 Colombrita, C., Zennaro, E., Fallini, C., Weber, M., Sommacal, A., Buratti, E., Silani, V., and
968 Ratti, A. (2009). TDP-43 is recruited to stress granules in conditions of oxidative insult. J
969 Neurochem *111*, 1051-1061. 10.1111/j.1471-4159.2009.06383.x.

970 Coyne, A.N., Lorenzini, I., Chou, C.C., Torvund, M., Rogers, R.S., Starr, A., Zaepfel, B.L., Levy,
971 J., Johannesmeyer, J., Schwartz, J.C., et al. (2017). Post-transcriptional Inhibition of Hsc70-
972 4/HSPA8 Expression Leads to Synaptic Vesicle Cycling Defects in Multiple Models of ALS. Cell
973 Rep *21*, 110-125. 10.1016/j.celrep.2017.09.028.

974 Coyne, A.N., Siddegowda, B.B., Estes, P.S., Johannesmeyer, J., Kovalik, T., Daniel, S.G.,
975 Pearson, A., Bowser, R., and Zarnescu, D.C. (2014). Futsch/MAP1B mRNA is a translational
976 target of TDP-43 and is neuroprotective in a Drosophila model of amyotrophic lateral sclerosis. J
977 Neurosci *34*, 15962-15974. 10.1523/JNEUROSCI.2526-14.2014.

978 Coyne, A.N., Yamada, S.B., Siddegowda, B.B., Estes, P.S., Zaepfel, B.L., Johannesmeyer,
979 J.S., Lockwood, D.B., Pham, L.T., Hart, M.P., Cassel, J.A., et al. (2015). Fragile X protein
980 mitigates TDP-43 toxicity by remodeling RNA granules and restoring translation. Hum Mol
981 Genet *24*, 6886-6898. 10.1093/hmg/ddv389.

982 Crittenden (1998). Tripartite Mushroom Body Architecture Revealed by Antigenic Markers.

983 de Belle, J.S., and Heisenberg, M. (1994). Associative odor learning in Drosophila abolished by
984 chemical ablation of mushroom bodies. Science *263*, 692-695. 10.1126/science.8303280.

985 Dennis, G., Jr., Sherman, B.T., Hosack, D.A., Yang, J., Gao, W., Lane, H.C., and Lempicki, R.A.
986 (2003). DAVID: Database for Annotation, Visualization, and Integrated Discovery. Genome Biol
987 *4*, P3.

988 Dobin, A., Davis, C.A., Schlesinger, F., Drenkow, J., Zaleski, C., Jha, S., Batut, P., Chaisson,
989 M., and Gingeras, T.R. (2013). STAR: ultrafast universal RNA-seq aligner. Bioinformatics *29*,
990 15-21. 10.1093/bioinformatics/bts635.

991 Driscoll, M., Buchert, S.N., Coleman, V., McLaughlin, M., Nguyen, A., and Sitaraman, D. (2021).
992 Compartment specific regulation of sleep by mushroom body requires GABA and dopaminergic
993 signaling. Sci Rep *11*, 20067. 10.1038/s41598-021-99531-2.

994 Elden, A.C., Kim, H.J., Hart, M.P., Chen-Plotkin, A.S., Johnson, B.S., Fang, X., Armakola, M.,
995 Geser, F., Greene, R., Lu, M.M., et al. (2010). Ataxin-2 intermediate-length polyglutamine
996 expansions are associated with increased risk for ALS. Nature *466*, 1069-1075.
997 10.1038/nature09320.

998 Enell, L.E., Kapan, N., Soderberg, J.A., Kahsai, L., and Nassel, D.R. (2010). Insulin signaling,
999 lifespan and stress resistance are modulated by metabotropic GABA receptors on insulin
1000 producing cells in the brain of Drosophila. PLoS One *5*, e15780. 10.1371/journal.pone.0015780.

1001 Erwin, D.H. (2015). Early metazoan life: divergence, environment and ecology. Philos Trans R
1002 Soc Lond B Biol Sci *370*. 10.1098/rstb.2015.0036.

1003 Estes, P.S., Boehringer, A., Zwick, R., Tang, J.E., Grigsby, B., and Zarnescu, D.C. (2011). Wild-
1004 type and A315T mutant TDP-43 exert differential neurotoxicity in a Drosophila model of ALS.
1005 Hum Mol Genet *20*, 2308-2321. 10.1093/hmg/ddr124.

1006 Estes, P.S., Daniel, S.G., McCallum, A.P., Boehringer, A.V., Sukhina, A.S., Zwick, R.A., and
1007 Zarnescu, D.C. (2013). Motor neurons and glia exhibit specific individualized responses to TDP-
1008 43 expression in a Drosophila model of amyotrophic lateral sclerosis. Dis Model Mech *6*, 721-
1009 733. 10.1242/dmm.010710.

1010 Fallini, C., Bassell, G.J., and Rossoll, W. (2012). The ALS disease protein TDP-43 is actively
1011 transported in motor neuron axons and regulates axon outgrowth. Hum Mol Genet *21*, 3703-
1012 3718. 10.1093/hmg/dds205.

1013 Feiguin, F., Godena, V.K., Romano, G., D'Ambrogio, A., Klima, R., and Baralle, F.E. (2009).
1014 Depletion of TDP-43 affects Drosophila motoneurons terminal synapsis and locomotive
1015 behavior. FEBS Lett *583*, 1586-1592. 10.1016/j.febslet.2009.04.019.

1016 Ferrari, R., Kapogiannis, D., Huey, E.D., and Momeni, P. (2011). FTD and ALS: a tale of two
1017 diseases. Curr Alzheimer Res *8*, 273-294. 10.2174/156720511795563700.

1018 Fiesel, F.C., Weber, S.S., Supper, J., Zell, A., and Kahle, P.J. (2012). TDP-43 regulates global
1019 translational yield by splicing of exon junction complex component SKAR. Nucleic Acids Res *40*,
1020 2668-2682. 10.1093/nar/gkr1082.

1021 Freibaum, B.D., Chitta, R.K., High, A.A., and Taylor, J.P. (2010). Global analysis of TDP-43
1022 interacting proteins reveals strong association with RNA splicing and translation machinery. J
1023 Proteome Res *9*, 1104-1120. 10.1021/pr901076y.

1024 Gao, J., Wang, L., Huntley, M.L., Perry, G., and Wang, X. (2018). Pathomechanisms of TDP-43
1025 in neurodegeneration. J Neurochem. 10.1111/jnc.14327.

1026 Gonzalez-Fernandez, C., Gonzalez, P., Andres-Benito, P., Ferrer, I., and Rodriguez, F.J.
1027 (2019). Wnt Signaling Alterations in the Human Spinal Cord of Amyotrophic Lateral Sclerosis
1028 Cases: Spotlight on Fz2 and Wnt5a. Mol Neurobiol *56*, 6777-6791. 10.1007/s12035-019-1547-
1029 9.

1030 Graham, A., Davies, R., Xuereb, J., Halliday, G., Kril, J., Creasey, H., Graham, K., and Hodges,
1031 J. (2005). Pathologically proven frontotemporal dementia presenting with severe amnesia. Brain
1032 *128*, 597-605. 10.1093/brain/awh348.

1033 Hampel, S., Chung, P., McKellar, C.E., Hall, D., Looger, L.L., and Simpson, J.H. (2011).
1034 Drosophila Brainbow: a recombinase-based fluorescence labeling technique to subdivide neural
1035 expression patterns. Nat Methods *8*, 253-259. 10.1038/nmeth.1566.

1036 Harbison, S.T., Serrano Negron, Y.L., Hansen, N.F., and Lobell, A.S. (2017). Selection for long
1037 and short sleep duration in Drosophila melanogaster reveals the complex genetic network
1038 underlying natural variation in sleep. PLoS Genet *13*, e1007098. 10.1371/journal.pgen.1007098.

1039 Hasegawa, M., Arai, T., Akiyama, H., Nonaka, T., Mori, H., Hashimoto, T., Yamazaki, M., and
1040 Oyanagi, K. (2007). TDP-43 is deposited in the Guam parkinsonism-dementia complex brains.
1041 Brain *130*, 1386-1394. 10.1093/brain/awm065.

1042 Heisenberg, M. (2003). Mushroom body memoir: from maps to models. Nat Rev Neurosci *4*,
1043 266-275. 10.1038/nrn1074.

1044 Hornberger, M., and Piguet, O. (2012). Episodic memory in frontotemporal dementia: a critical
1045 review. Brain *135*, 678-692. 10.1093/brain/aws011.

1046 Isabel, G., Pascual, A., and Preat, T. (2004). Exclusive consolidated memory phases in
1047 Drosophila. Science *304*, 1024-1027. 10.1126/science.1094932.

1048 Ito, K., Awano, W., Suzuki, K., Hiromi, Y., and Yamamoto, D. (1997). The Drosophila mushroom
1049 body is a quadruple structure of clonal units each of which contains a virtually identical set of
1050 neurones and glial cells. Development *124*, 761-771. 10.1242/dev.124.4.761.

1051 Jo, M., Lee, S., Jeon, Y.M., Kim, S., Kwon, Y., and Kim, H.J. (2020). The role of TDP-43
1052 propagation in neurodegenerative diseases: integrating insights from clinical and experimental
1053 studies. Exp Mol Med *52*, 1652-1662. 10.1038/s12276-020-00513-7.

1054 Joiner, W.J., Crocker, A., White, B.H., and Sehgal, A. (2006). Sleep in Drosophila is regulated
1055 by adult mushroom bodies. Nature *441*, 757-760. 10.1038/nature04811.

1056 Josephs, K.A., Murray, M.E., Whitwell, J.L., Parisi, J.E., Petrucelli, L., Jack, C.R., Petersen,
1057 R.C., and Dickson, D.W. (2014a). Staging TDP-43 pathology in Alzheimer's disease. Acta
1058 Neuropathol *127*, 441-450. 10.1007/s00401-013-1211-9.

1059 Josephs, K.A., Whitwell, J.L., Weigand, S.D., Murray, M.E., Tosakulwong, N., Liesinger, A.M.,
1060 Petrucelli, L., Senjem, M.L., Knopman, D.S., Boeve, B.F., et al. (2014b). TDP-43 is a key player
1061 in the clinical features associated with Alzheimer's disease. Acta Neuropathol *127*, 811-824.
1062 10.1007/s00401-014-1269-z.

1063 Kabashi, E., Valdmanis, P.N., Dion, P., Spiegelman, D., McConkey, B.J., Vande Velde, C.,
1064 Bouchard, J.P., Lacomblez, L., Pochigaeva, K., Salachas, F., et al. (2008). TARDBP mutations
1065 in individuals with sporadic and familial amyotrophic lateral sclerosis. Nat Genet *40*, 572-574.
1066 10.1038/ng.132.

1067 Kamyshev, N.G., Smirnova, G.P., Kamysheva, E.A., Nikiforov, O.N., Parafenyuk, I.V., and
1068 Ponomarenko, V.V. (2002). Plasticity of social behavior in Drosophila. Neurosci Behav Physiol
1069 *32*, 401-408. 10.1023/a:1015832328023.

1070 Kansal, K., Mareddy, M., Sloane, K.L., Minc, A.A., Rabins, P.V., McGready, J.B., and Onyike,
1071 C.U. (2016). Survival in Frontotemporal Dementia Phenotypes: A Meta-Analysis. Dement
1072 Geriatr Cogn Disord *41*, 109-122. 10.1159/000443205.

1073 Kassambara, A. (2020). ggpubr: 'ggplot2' Based Publication Ready Plots.

1074 Kassambara, A., Kosinski, M., and Biecek, P. (2021). survminer: Drawing Survival Curves using
1075 'ggplot2'. R package version 0.4.9.

1076 Khalfallah, Y., Kuta, R., Grasmuck, C., Prat, A., Durham, H.D., and Vande Velde, C. (2018).
1077 TDP-43 regulation of stress granule dynamics in neurodegenerative disease-relevant cell types.
1078 Sci Rep *8*, 7551. 10.1038/s41598-018-25767-0.

1079 Kunz, T., Kraft, K.F., Technau, G.M., and Urbach, R. (2012). Origin of Drosophila mushroom
1080 body neuroblasts and generation of divergent embryonic lineages. Development *139*, 2510-
1081 2522. 10.1242/dev.077883.

1082 Langellotti, S., Romano, G., Feiguin, F., Baralle, F.E., and Romano, M. (2018). RhoGAPp190: A
1083 potential player in tbph-mediated neurodegeneration in Drosophila. PLoS One *13*, e0195845.
1084 10.1371/journal.pone.0195845.

1085 Lee, T., Lee, A., and Luo, L. (1999). Development of the Drosophila mushroom bodies:
1086 sequential generation of three distinct types of neurons from a neuroblast. Development *126*,
1087 4065-4076. 10.1242/dev.126.18.4065.

1088 Lehmkuhl, E.M., Loganathan, S., Alsop, E., Blythe, A.D., Kovalik, T., Mortimore, N.P.,
1089 Barrameda, D., Kueth, C., Eck, R.J., Siddegowda, B.B., et al. (2021). TDP-43 proteinopathy
1090 alters the ribosome association of multiple mRNAs including the glypican Dally-like protein
1091 (Dlp)/GPC6. Acta Neuropathol Commun *9*, 52. 10.1186/s40478-021-01148-z.

1092 Lewis, S.A., Negelspach, D.C., Kaladchibachi, S., Cowen, S.L., and Fernandez, F. (2017).
1093 Spontaneous alternation: A potential gateway to spatial working memory in Drosophila.
1094 Neurobiol Learn Mem *142*, 230-235. 10.1016/j.nlm.2017.05.013.

1095 Li, J., Vitiello, M.V., and Gooneratne, N.S. (2018). Sleep in Normal Aging. Sleep Med Clin *13*, 1-
1096 11. 10.1016/j.jsmc.2017.09.001.

1097 Li, Y., Ray, P., Rao, E.J., Shi, C., Guo, W., Chen, X., Woodruff, E.A., 3rd, Fushimi, K., and Wu,
1098 J.Y. (2010). A Drosophila model for TDP-43 proteinopathy. Proc Natl Acad Sci U S A *107*, 3169-
1099 3174. 10.1073/pnas.0913602107.

1100 Liao, Y., Smyth, G.K., and Shi, W. (2014). featureCounts: an efficient general purpose program
1101 for assigning sequence reads to genomic features. Bioinformatics *30*, 923-930.
1102 10.1093/bioinformatics/btt656.

1103 Lien, W.Y., Chen, Y.T., Li, Y.J., Wu, J.K., Huang, K.L., Lin, J.R., Lin, S.C., Hou, C.C., Wang,
1104 H.D., Wu, C.L., et al. (2020). Lifespan regulation in alpha/beta posterior neurons of the fly
1105 mushroom bodies by Rab27. Aging Cell *19*, e13179. 10.1111/acel.13179.

1106 Ling, J.P., Pletnikova, O., Troncoso, J.C., and Wong, P.C. (2015). TDP-43 repression of
1107 nonconserved cryptic exons is compromised in ALS-FTD. Science *349*, 650-655.
1108 10.1126/science.aab0983.

1109 Ling, S.C., Polymenidou, M., and Cleveland, D.W. (2013). Converging mechanisms in ALS and
1110 FTD: disrupted RNA and protein homeostasis. Neuron *79*, 416-438.
1111 10.1016/j.neuron.2013.07.033.

1112 Liu, L., Wolf, R., Ernst, R., and Heisenberg, M. (1999). Context generalization in Drosophila
1113 visual learning requires the mushroom bodies. Nature *400*, 753-756. 10.1038/23456.

1114 Loganathan, S., Wilson, B.A., Carey, S.B., Manzo, E., Joardar, A., Ugur, B., and Zarnescu, D.C.
1115 (2022). TDP-43 Proteinopathy Causes Broad Metabolic Alterations including TCA Cycle
1116 Intermediates and Dopamine Levels in Drosophila Models of ALS. Metabolites *12*.
1117 10.3390/metabo12020101.

1118 Loi, S.M., Tsoukra, P., Chen, Z., Wibawa, P., Eratne, D., Kelso, W., Walterfang, M., and
1119 Velakoulis, D. (2021). Risk factors to mortality and causes of death in frontotemporal dementia:
1120 An Australian perspective. Int J Geriatr Psychiatry *37*. 10.1002/gps.5668.

1121 Love, M.I., Huber, W., and Anders, S. (2014). Moderated estimation of fold change and
1122 dispersion for RNA-seq data with DESeq2. Genome Biol *15*, 550. 10.1186/s13059-014-0550-8.

1123 Lu, Y., Ferris, J., and Gao, F.B. (2009). Frontotemporal dementia and amyotrophic lateral
1124 sclerosis-associated disease protein TDP-43 promotes dendritic branching. Mol Brain *2*, 30.
1125 10.1186/1756-6606-2-30.

1126 Mackenzie, I.R., Bigio, E.H., Ince, P.G., Geser, F., Neumann, M., Cairns, N.J., Kwong, L.K.,
1127 Forman, M.S., Ravits, J., Stewart, H., et al. (2007). Pathological TDP-43 distinguishes sporadic
1128 amyotrophic lateral sclerosis from amyotrophic lateral sclerosis with SOD1 mutations. Ann
1129 Neurol *61*, 427-434. 10.1002/ana.21147.

1130 Mackenzie, I.R., Neumann, M., Baborie, A., Sampathu, D.M., Du Plessis, D., Jaros, E., Perry,
1131 R.H., Trojanowski, J.Q., Mann, D.M., and Lee, V.M. (2011). A harmonized classification system
1132 for FTLD-TDP pathology. Acta Neuropathol *122*, 111-113. 10.1007/s00401-011-0845-8.

1133 Mackenzie, I.R.A., Rademakers, R., and Neumann, M. (2010). TDP-43 and FUS in amyotrophic
1134 lateral sclerosis and frontotemporal dementia. The Lancet Neurology *9*, 995-1007.
1135 10.1016/s1474-4422(10)70195-2.

1136 Manzo, E., Lorenzini, I., Barrameda, D., O'Conner, A.G., Barrows, J.M., Starr, A., Kovalik, T.,
1137 Rabichow, B.E., Lehmkuhl, E.M., Shreiner, D.D., et al. (2019). Glycolysis upregulation is
1138 neuroprotective as a compensatory mechanism in ALS. Elife *8*. 10.7554/eLife.45114.

1139 Mariano, V., Achsel, T., Bagni, C., and Kanellopoulos, A.K. (2020). Modelling Learning and
1140 Memory in Drosophila to Understand Intellectual Disabilities. Neuroscience *445*, 12-30.
1141 10.1016/j.neuroscience.2020.07.034.

1142 McAleese, K.E., Walker, L., Erskine, D., Thomas, A.J., McKeith, I.G., and Attems, J. (2017).
1143 TDP-43 pathology in Alzheimer's disease, dementia with Lewy bodies and ageing. Brain Pathol
1144 *27*, 472-479. 10.1111/bpa.12424.

1145 McCarter, S.J., St Louis, E.K., and Boeve, B.F. (2016). Sleep Disturbances in Frontotemporal
1146 Dementia. Curr Neurol Neurosci Rep *16*, 85. 10.1007/s11910-016-0680-3.

1147 McDonald, K.K., Aulas, A., Destroismaisons, L., Pickles, S., Beleac, E., Camu, W., Rouleau,
1148 G.A., and Vande Velde, C. (2011). TAR DNA-binding protein 43 (TDP-43) regulates stress
1149 granule dynamics via differential regulation of G3BP and TIA-1. Human Molecular Genetics *20*,
1150 1400-1410. 10.1093/hmg/ddr021.

1151 Meneses, A., Koga, S., O'Leary, J., Dickson, D.W., Bu, G., and Zhao, N. (2021). TDP-43
1152 Pathology in Alzheimer's Disease. Mol Neurodegener *16*, 84. 10.1186/s13024-021-00503-x.

1153 Mershin, A., Pavlopoulos, E., Fitch, O., Braden, B.C., Nanopoulos, D.V., and Skoulakis, E.M.
1154 (2004). Learning and memory deficits upon TAU accumulation in Drosophila mushroom body
1155 neurons. Learn Mem *11*, 277-287. 10.1101/lm.70804.

1156 Morante, J., and Desplan, C. (2008). The color-vision circuit in the medulla of Drosophila. Curr
1157 Biol *18*, 553-565. 10.1016/j.cub.2008.02.075.

1158 Muqit, M.M., and Feany, M.B. (2002). Modelling neurodegenerative diseases in Drosophila: a
1159 fruitful approach? Nat Rev Neurosci *3*, 237-243. 10.1038/nrn751.

1160 Murley, A.G., and Rowe, J.B. (2018). Neurotransmitter deficits from frontotemporal lobar
1161 degeneration. Brain *141*, 1263-1285. 10.1093/brain/awx327.

1162 Murphy, S.L., Kochanek, K.D., Xu, J., and Aria, E. (2021). Mortality in the United States, 2020.
1163 U.S. Department of Health and Human Services.
1164 https://www.cdc.gov/nchs/data/databriefs/db427.pdf.

1165 Nana, A.L., Sidhu, M., Gaus, S.E., Hwang, J.L., Li, L., Park, Y., Kim, E.J., Pasquini, L., Allen,
1166 I.E., Rankin, K.P., et al. (2019). Neurons selectively targeted in frontotemporal dementia reveal
1167 early stage TDP-43 pathobiology. Acta Neuropathol *137*, 27-46. 10.1007/s00401-018-1942-8.

1168 Neumann, M., Sampathu, D.M., Kwong, L.K., Truax, A.C., Micsenyi, M.C., Chou, T.T., Bruce, J.,
1169 Schuck, T., Grossman, M., Clark, C.M., et al. (2006). Ubiquitinated TDP-43 in frontotemporal
1170 lobar degeneration and amyotrophic lateral sclerosis. Science *314*, 130-133.
1171 10.1126/science.1134108.

1172 Ostrowski, D., Kahsai, L., Kramer, E.F., Knutson, P., and Zars, T. (2015). Place memory
1173 retention in Drosophila. Neurobiol Learn Mem *123*, 217-224. 10.1016/j.nlm.2015.06.015.

1174 Park, J.H., Chung, C.G., Park, S.S., Lee, D., Kim, K.M., Jeong, Y., Kim, E.S., Cho, J.H., Jeon,
1175 Y.-M., Shen, C.K.J., et al. (2020). Cytosolic calcium regulates cytoplasmic accumulation of TDP-
1176 43 through Calpain-A and Importin α3. eLife *9*, e60132. 10.7554/eLife.60132.

1177 Pennington, C., Hodges, J.R., and Hornberger, M. (2011). Neural correlates of episodic memory
1178 in behavioral variant frontotemporal dementia. J Alzheimers Dis *24*, 261-268. 10.3233/JAD-
1179 2011-101668.

1180 Perry, D.C., Brown, J.A., Possin, K.L., Datta, S., Trujillo, A., Radke, A., Karydas, A., Kornak, J.,
1181 Sias, A.C., Rabinovici, G.D., et al. (2017). Clinicopathological correlations in behavioural variant
1182 frontotemporal dementia. Brain *140*, 3329-3345. 10.1093/brain/awx254.

1183 Polymenidou, M., Lagier-Tourenne, C., Hutt, K.R., Huelga, S.C., Moran, J., Liang, T.Y., Ling, S.-
1184 C., Sun, E., Wancewicz, E., Mazur, C., et al. (2011). Long pre-mRNA depletion and RNA
1185 missplicing contribute to neuronal vulnerability from loss of TDP-43. Nature Neuroscience *14*,
1186 459-468. 10.1038/nn.2779.

1187 Poos, J.M., Jiskoot, L.C., Papma, J.M., van Swieten, J.C., and van den Berg, E. (2018). Meta-
1188 analytic Review of Memory Impairment in Behavioral Variant Frontotemporal Dementia. J Int
1189 Neuropsychol Soc *24*, 593-605. 10.1017/S1355617718000115.

1190 Ramaswami, M., Taylor, J.P., and Parker, R. (2013). Altered Ribostasis: RNA-Protein Granules
1191 in Degenerative Disorders. Cell *154*, 727-736. 10.1016/j.cell.2013.07.038.

1192 Rascovsky, K., Hodges, J.R., Knopman, D., Mendez, M.F., Kramer, J.H., Neuhaus, J., van
1193 Swieten, J.C., Seelaar, H., Dopper, E.G., Onyike, C.U., et al. (2011). Sensitivity of revised
1194 diagnostic criteria for the behavioural variant of frontotemporal dementia. Brain *134*, 2456-2477.
1195 10.1093/brain/awr179.

1196 Rawson, J.M., Dimitroff, B., Johnson, K.G., Rawson, J.M., Ge, X., Van Vactor, D., and Selleck,
1197 S.B. (2005). The heparan sulfate proteoglycans Dally-like and Syndecan have distinct functions
1198 in axon guidance and visual-system assembly in Drosophila. Curr Biol *15*, 833-838.
1199 10.1016/j.cub.2005.03.039.

1200 Rohn, T.T. (2008). Caspase-cleaved TAR DNA-binding protein-43 is a major pathological
1201 finding in Alzheimer's disease. Brain Research *1228*, 189-198. 10.1016/j.brainres.2008.06.094.

1202 Romano, M., Feiguin, F., and Buratti, E. (2012). Drosophila Answers to TDP-43
1203 Proteinopathies. J Amino Acids *2012*, 356081. 10.1155/2012/356081.

1204 Rutherford, N.J., Zhang, Y.J., Baker, M., Gass, J.M., Finch, N.A., Xu, Y.F., Stewart, H., Kelley,
1205 B.J., Kuntz, K., Crook, R.J., et al. (2008). Novel mutations in TARDBP (TDP-43) in patients with
1206 familial amyotrophic lateral sclerosis. PLoS Genet *4*, e1000193. 10.1371/journal.pgen.1000193.

1207 Sani, T.P., Bond, R.L., Marshall, C.R., Hardy, C.J.D., Russell, L.L., Moore, K.M., Slattery, C.F.,
1208 Paterson, R.W., Woollacott, I.O.C., Wendi, I.P., et al. (2019). Sleep symptoms in syndromes of
1209 frontotemporal dementia and Alzheimer's disease: A proof-of-principle behavioural study.
1210 eNeurologicalSci *17*, 100212. 10.1016/j.ensci.2019.100212.

1211 Santiago, J.A., Bottero, V., and Potashkin, J.A. (2020). Transcriptomic and Network Analysis
1212 Identifies Shared and Unique Pathways across Dementia Spectrum Disorders. Int J Mol Sci *21*.
1213 10.3390/ijms21062050.

1214 Seeley, W.W. (2008). Selective functional, regional, and neuronal vulnerability in frontotemporal
1215 dementia. Curr Opin Neurol *21*, 701-707. 10.1097/WCO.0b013e3283168e2d.

1216 Shaw, P.J., Cirelli, C., Greenspan, R.J., and Tononi, G. (2000). Correlates of sleep and waking
1217 in Drosophila melanogaster. Science *287*, 1834-1837. 10.1126/science.287.5459.1834.

1218 Sherman, B.T., Hao, M., Qiu, J., Jiao, X., Baseler, M.W., Lane, H.C., Imamichi, T., and Chang,
1219 W. (2022). DAVID: a web server for functional enrichment analysis and functional annotation of
1220 gene lists (2021 update). Nucleic Acids Res *50*, W216-221. 10.1093/nar/gkac194.

1221 Sreedharan, J., Blair, I.P., Tripathi, V.B., Hu, X., Vance, C., Rogelj, B., Ackerley, S., Durnall,
1222 J.C., Williams, K.L., Buratti, E., et al. (2008). TDP-43 Mutations in Familial and Sporadic
1223 Amyotrophic Lateral Sclerosis. Science *319*, 1668-1672. 10.1126/science.1154584.

1224 Sreedharan, J., Neukomm, L.J., Brown, R.H., Jr., and Freeman, M.R. (2015). Age-Dependent
1225 TDP-43-Mediated Motor Neuron Degeneration Requires GSK3, hat-trick, and xmas-2. Curr Biol
1226 *25*, 2130-2136. 10.1016/j.cub.2015.06.045.

1227 Stewart, B.A., Atwood, H.L., Renger, J.J., Wang, J., and Wu, C.F. (1994). Improved stability of
1228 Drosophila larval neuromuscular preparations in haemolymph-like physiological solutions. J
1229 Comp Physiol A *175*, 179-191. 10.1007/BF00215114.

1230 Stopford, C.L., Thompson, J.C., Neary, D., Richardson, A.M., and Snowden, J.S. (2012).
1231 Working memory, attention, and executive function in Alzheimer's disease and frontotemporal
1232 dementia. Cortex *48*, 429-446. 10.1016/j.cortex.2010.12.002.

1233 Strausfeld, N.J., and Hirth, F. (2013). Deep homology of arthropod central complex and
1234 vertebrate basal ganglia. Science *340*, 157-161. 10.1126/science.1231828.

1235 Sun, Y., Qiu, R., Li, X., Cheng, Y., Gao, S., Kong, F., Liu, L., and Zhu, Y. (2020). Social
1236 attraction in Drosophila is regulated by the mushroom body and serotonergic system. Nat
1237 Commun *11*, 5350. 10.1038/s41467-020-19102-3.

1238 Susnjar, U., Skrabar, N., Brown, A.L., Abbassi, Y., Phatnani, H., Consortium, N.A., Cortese, A.,
1239 Cereda, C., Bugiardini, E., Cardani, R., et al. (2022). Cell environment shapes TDP-43 function
1240 with implications in neuronal and muscle disease. Commun Biol *5*, 314. 10.1038/s42003-022-
1241 03253-8.

1242 Swain, A., Misulovin, Z., Pherson, M., Gause, M., Mihindukulasuriya, K., Rickels, R.A.,
1243 Shilatifard, A., and Dorsett, D. (2016). Drosophila TDP-43 RNA-Binding Protein Facilitates
1244 Association of Sister Chromatid Cohesion Proteins with Genes, Enhancers and Polycomb
1245 Response Elements. PLoS Genet *12*, e1006331. 10.1371/journal.pgen.1006331.

1246 Team, R. (2022). RStudio: Integrated Development Environment for R. (PBC).

1247 Team, R.C. (2021). A language and environment for statistical computing. (R Foundation for
1248 Statistical Computing).

1249 Therneau, T.M. (2021). _A Package for Survival Analysis in R_. R package version
1250 3.2-13.

1251 Tollervey, J.R., Curk, T., Rogelj, B., Briese, M., Cereda, M., Kayikci, M., König, J., Hortobágyi,
1252 T., Nishimura, A.L., Župunski, V., et al. (2011). Characterizing the RNA targets and position-
1253 dependent splicing regulation by TDP-43. Nature Neuroscience *14*, 452-458. 10.1038/nn.2778.

1254 Tsao, C.H., Chen, C.C., Lin, C.H., Yang, H.Y., and Lin, S. (2018). Drosophila mushroom bodies
1255 integrate hunger and satiety signals to control innate food-seeking behavior. Elife *7*.
1256 10.7554/eLife.35264.

1257 Vogt, K., Schnaitmann, C., Dylla, K.V., Knapek, S., Aso, Y., Rubin, G.M., and Tanimoto, H.
1258 (2014). Shared mushroom body circuits underlie visual and olfactory memories in Drosophila.
1259 Elife *3*, e02395. 10.7554/eLife.02395.

1260 Waghmare, I., Wang, X., and Page-McCaw, A. (2020). Dally-like protein sequesters multiple
1261 Wnt ligands in the Drosophila germarium. Dev Biol *464*, 88-102. 10.1016/j.ydbio.2020.05.004.

1262 Walker, A.K., Spiller, K.J., Ge, G., Zheng, A., Xu, Y., Zhou, M., Tripathy, K., Kwong, L.K.,
1263 Trojanowski, J.Q., and Lee, V.M.Y. (2015). Functional recovery in new mouse models of
1264 ALS/FTLD after clearance of pathological cytoplasmic TDP-43. Acta Neuropathologica *130*,
1265 643-660. 10.1007/s00401-015-1460-x.

1266 Wickham, H., Averick, M., Bryan, J., Chang, W., McGowan, L., François, R., Grolemund, G.,
1267 Hayes, A., Henry, L., Hester, J., et al. (2019). Welcome to the Tidyverse. Journal of Open
1268 Source Software *4*. 10.21105/joss.01686.

1269 Wolff, G.H., and Strausfeld, N.J. (2016). Genealogical correspondence of a forebrain centre
1270 implies an executive brain in the protostome-deuterostome bilaterian ancestor. Philos Trans R
1271 Soc Lond B Biol Sci *371*, 20150055. 10.1098/rstb.2015.0055.

1272 Xiao, S., Sanelli, T., Dib, S., Sheps, D., Findlater, J., Bilbao, J., Keith, J., Zinman, L., Rogaeva,
1273 E., and Robertson, J. (2011). RNA targets of TDP-43 identified by UV-CLIP are deregulated in
1274 ALS. Mol Cell Neurosci *47*, 167-180. 10.1016/j.mcn.2011.02.013.

1275 Yamazaki, D., Horiuchi, J., Nakagami, Y., Nagano, S., Tamura, T., and Saitoe, M. (2007). The
1276 Drosophila DCO mutation suppresses age-related memory impairment without affecting
1277 lifespan. Nat Neurosci *10*, 478-484. 10.1038/nn1863.

1278 Yan, D., Wu, Y., Feng, Y., Lin, S.C., and Lin, X. (2009). The core protein of glypican Dally-like
1279 determines its biphasic activity in wingless morphogen signaling. Dev Cell *17*, 470-481.
1280 10.1016/j.devcel.2009.09.001.

1281 Yu, H.H., and Lee, T. (2007). Neuronal temporal identity in post-embryonic Drosophila brain.
1282 Trends Neurosci *30*, 520-526. 10.1016/j.tins.2007.07.003.

1283 Zhan, L., Hanson, K.A., Kim, S.H., Tare, A., and Tibbetts, R.S. (2013). Identification of genetic
1284 modifiers of TDP-43 neurotoxicity in Drosophila. PLoS One *8*, e57214.
1285 10.1371/journal.pone.0057214.

1286 Zhang, K., Guo, J.Z., Peng, Y., Xi, W., and Guo, A. (2007). Dopamine-mushroom body circuit
1287 regulates saliency-based decision-making in Drosophila. Science *316*, 1901-1904.
1288 10.1126/science.1137357.

1289 Zwarts, L., Vanden Broeck, L., Cappuyns, E., Ayroles, J.F., Magwire, M.M., Vulsteke, V.,
1290 Clements, J., Mackay, T.F., and Callaerts, P. (2015). The genetic basis of natural variation in
1291 mushroom body size in Drosophila melanogaster. Nat Commun *6*, 10115.
1292 10.1038/ncomms10115.
1293